



UNIVERSITY OF LEEDS

This is a repository copy of *Anti-PD-1/anti-CTLA-4 efficacy in melanoma brain metastases depends on extracranial disease and augmentation of CD8+ T cell trafficking*.

White Rose Research Online URL for this paper:
<http://eprints.whiterose.ac.uk/127020/>

Version: Accepted Version

Article:

Taggart, D, Andreou, T, Scott, KJ orcid.org/0000-0002-5790-9579 et al. (7 more authors) (2018) Anti-PD-1/anti-CTLA-4 efficacy in melanoma brain metastases depends on extracranial disease and augmentation of CD8+ T cell trafficking. *Proceedings of the National Academy of Sciences of the United States of America*, 115 (7). E1540-E1549. ISSN 0027-8424

<https://doi.org/10.1073/pnas.1714089115>

(c) 2018. Published under the PNAS license [<http://www.pnas.org/page/authors/licenses>]. This is an author produced version of a paper published in the *Proceedings of the National Academy of Sciences*. Uploaded in accordance with the publisher's self-archiving policy. In order to comply with the publisher requirements the University does not require the author to sign a non-exclusive licence for this paper.

Reuse

Items deposited in White Rose Research Online are protected by copyright, with all rights reserved unless indicated otherwise. They may be downloaded and/or printed for private study, or other acts as permitted by national copyright laws. The publisher or other rights holders may allow further reproduction and re-use of the full text version. This is indicated by the licence information on the White Rose Research Online record for the item.

Takedown

If you consider content in White Rose Research Online to be in breach of UK law, please notify us by emailing eprints@whiterose.ac.uk including the URL of the record and the reason for the withdrawal request.



eprints@whiterose.ac.uk
<https://eprints.whiterose.ac.uk/>

Major category: Biological sciences

Minor categories: Immunology and inflammation, cell biology

Anti-PD-1/anti-CTLA-4 efficacy in melanoma brain metastases depends on extracranial disease and augmentation of CD8+ T cell trafficking

David Taggart^{a,b}, Tereza Andreou^a, Karen J. Scott^a, Jennifer Williams^a, Nora Rippaus^a, Rebecca J. Brownlie^a, Elizabeth J. Ilett^a, Robert J. Salmond^a, Alan Melcher^{a,c}, Mihaela Lorger^{a1}

^aLeeds Institute of Cancer and Pathology, University of Leeds, Leeds, UK.

^bMRC Centre for Inflammation research, The University of Edinburgh, Edinburgh, UK.

^cThe Institute of Cancer Research and The Royal Marsden NHS Foundation Trust, London, UK.

¹To whom correspondence should be addressed:

Mihaela Lorger, PhD

Leeds Institute of Cancer and Pathology

University of Leeds

Wellcome Trust Brenner Building

St. James's University Hospital

Beckett Street

LS9 7TF Leeds

UK

0044 (0)113 343 8449

M.Lorger@leeds.ac.uk

A short title: Anti-PD-1/anti-CTLA-4 therapy in brain metastases

Keywords: anti-PD-1, anti-CTLA-4, melanoma, brain metastases, T cell trafficking

The authors declare no conflict of interest.

Abstract

Inhibition of immune checkpoints Programmed Death 1 (PD-1) and Cytotoxic T-lymphocyte Associated Protein 4 (CTLA-4) on T cells results in durable anti-tumor activity in melanoma patients. Despite high frequency of melanoma brain metastases (BrM) and associated poor prognosis, the activity and mechanisms of immune checkpoint inhibitors (ICI) in metastatic tumors that develop within the “immune specialized” brain microenvironment, remain elusive. We established a melanoma tumor transplantation model with intracranial plus extracranial (subcutaneous) tumor, mimicking the clinically observed coexistence of metastases inside and outside the brain. Strikingly, intracranial ICI efficacy was observed only when extracranial tumor was present. Extracranial tumor was also required for ICI-induced increase in CD8⁺ T cells, macrophages and microglia in brain tumors, as well as for upregulation of immune-regulatory genes. Combined PD-1/CTLA-4 blockade had a superior intracranial efficacy over the two monotherapies. Cell depletion studies revealed that NK cells and CD8⁺ T cells were required for intracranial anti-PD-1/anti-CTLA-4 efficacy. Rather than enhancing CD8⁺ T cell activation and expansion within intracranial tumors, PD-1/CTLA-4 blockade dramatically (~14-fold) increased the trafficking of CD8⁺ T cells to the brain. This was mainly through the peripheral expansion of homing-competent effector CD8⁺ T cells and potentially further enhanced through upregulation of T cell entry receptors ICAM-1 and VCAM-1 on tumor vasculature. Our study indicates that extracranial activation/release of CD8⁺ T cells from PD-1/CTLA-4 inhibition and potentiation of their recruitment to the brain are paramount to the intracranial anti-PD-1/anti-CTLA-4 activity, suggesting augmentation of these processes as an immune therapy-enhancing strategy in metastatic brain cancer.

Significance statement:

Brain metastases are an unmet clinical need with high frequency in melanoma patients. With immune checkpoint inhibitors targeting PD-1 and CTLA-4 becoming a frontline therapy in melanoma, it is critical to understand how this therapy works in the “immune-specialized” brain microenvironment. Our study shows that in the absence of extracranial tumor, melanoma tumors growing in the brain escape anti-PD-1/anti-CTLA-4 therapy. A synergy between immune checkpoint inhibition and extracranial tumor is required to put a break on brain metastases by enhancing CD8+ T cell recruitment to the brain via peripheral expansion of effector cells and upregulation of T cell entry receptors on tumor blood vessels. Augmentation of these processes could be explored to enhance the efficacy of immunotherapy in brain metastases.

“\body”

Introduction

Brain metastases (BrM) are an unmet clinical need with very limited treatment options and poor prognosis. Metastatic melanoma has the highest risk of spreading to the central nervous system (CNS) among common cancers; up to a quarter of patients have BrM at metastatic diagnosis, and the incidence at autopsy is up to ~75% (1-3). Until recently, treatment options for melanoma BrM have been restricted to radiotherapy, surgery, and targeted therapies, with the median overall survival below one year (4, 5). In recent years, cancer treatment has been revolutionized by immunotherapy targeting PD-1 and CTLA-4 immune-inhibitory receptors (immune checkpoints) expressed mainly on T cells. Function-blocking antibodies against CTLA-4 (ipilimumab) and PD-1 (nivolumab, pembrolizumab) enhance anti-tumor T cell responses and result in durable anti-tumor activity across most cancers (6, 7). In melanoma, the anti-PD-1/anti-CTLA-4 combination therapy showed a superior efficacy as compared to the two monotherapies (8), and has been approved in various countries (9). Despite numerous studies on anti-PD-1 and anti-CTLA-4 in melanoma, very limited data are available for BrM, mainly due to frequent exclusion of patients with BrM from clinical trials (4, 10). A handful of retrospective and prospective clinical studies indicated activity of ipilimumab in melanoma BrM with 16-25% intracranial response rate, but also suggested that only a subgroup of patients is likely to benefit (4, 5, 11). Pembrolizumab and nivolumab also showed efficacy in melanoma BrM with an ~21% response rate in the brain (12-15). A very recent interim analyses from two clinical trials in drug-treatment naïve patients with melanoma BrM (ABC trial (15) and CheckMate 204 trial (16)) reported a 50% and 55% intracranial response rate following combined anti-PD-1 plus anti-CTLA-4 therapy.

In addition to limited clinical data, there is a complete lack of preclinical data on anti-PD-1 and anti-CTLA-4 therapy in melanoma BrM. Preclinical studies in BrM are hampered by the lack of melanoma models that can recapitulate clinically observed metastatic patterns and coexistence of metastases in different organs. Spontaneous metastasis to the brain in preclinical models is a rare event and macroscopic BrM are usually not observed (17). Only two immunocompetent pre-clinical melanoma models of spontaneous BrM have been reported (18, 19), but analysis of BrM-specific survival in therapeutic studies remains a challenge due to a faster development of extracranial as compared to intracranial metastases.

Notably, differences in regulation of adaptive T cell responses to antigens located in the CNS as compared to antigens outside the CNS have been well documented (20-24). Due to this difference in adaptive immune responses, the CNS has been referred to as “immune specialized”. Moreover, the phenotype of immune cells infiltrating brain metastases has been shown to be altered by inflammatory molecules upregulated specifically in cancer cells growing in the brain parenchyma (25). Hence, with immune checkpoint inhibitors (ICI) now being frontline therapy for metastatic melanoma, the question arises as to what extent the metastatic tumors residing within the immune specialized brain microenvironment respond to ICI. Moreover, the requirements for effective anti-PD-1/anti-CTLA-4 therapy in the brain remain to be identified.

To address the above knowledge gaps and study anti-PD-1/anti-CTLA-4-dependent survival and mechanisms specifically in BrM while simulating the clinically observed coexistence of metastasis in the skin (the most common metastatic site (26)), we established a melanoma transplantation model with extracranial (subcutaneous) plus intracranial tumors, in which the overall survival depends on the intracranial tumor growth. In addition to demonstrating a superior intracranial efficacy of combined PD-1/CTLA-4 blockade over the two monotherapies, we made a striking observation that anti-PD-1/anti-CTLA-4 activity in the brain depends on the presence of extracranial tumor, highlighting the importance of mimicking clinically observed extracranial disease in the context of ICI studies. We further show that the intracranial activity of anti-PD-1/anti-CTLA-4 therapy requires the augmentation of CD8⁺ T cell trafficking to the brain and we analyze the underlying mechanisms.

Results

The presence of extracranial tumor is critical for intracranial anti-PD-1/anti-CTLA-4 efficacy

The vast majority of BrM in melanoma coincide with metastases outside the brain, predominantly in the skin (26). To mimic this clinical situation, we established a tumor transplantation model of B16 melanoma with extracranial (subcutaneous) plus intracranial tumors. To identify the optimal experimental timeline allowing us to study survival specifically in dependence of intracranial tumor growth, we first determined tumor growth kinetics and survival times in mice bearing either extracranial or intracranial tumors (**Fig. 1A; Supplemental Fig. 1A, B**). The mean survival time for mice with intracranial tumors was 10.8 ± 1.5 days. Extracranial tumors reached the maximum allowable diameter of 15 mm on day 16.5 ± 1.4 and none of the mice showed terminal symptoms at this time point. Thus, subcutaneous (s.c.) implantation of cancer cells into the flank 3 days prior to their intracranial implantation (**Fig. 1B**) allowed for quantification of the intracranial tumor-dependent survival.

Following administration of 4 doses of either anti-CTLA-4 or anti-PD-1 antibody monotherapy (**Fig. 1B**), the overall survival of mice in this model was only marginally and non-significantly extended as compared to control mice receiving IgG isotype antibody (**Fig. 1C, Supplemental Fig. 1C**). In contrast to monotherapies, the anti-PD-1/anti-CTLA-4 combination significantly prolonged survival in our model and inhibited intracranial as well as extracranial tumor growth (**Fig. 1C-E, Supplemental Fig. 1C**). Thus, the outcome of anti-PD-1/anti-CTLA-4 combination therapy was superior to the two monotherapies, which is in line with the reported intracranial response rate for anti-PD-1 monotherapy (21-25%) (12-15) and anti-PD-1/anti-CTLA-4 combination therapy (50-55%) (15, 16), as well as the 6 month progression-free survival rate of 28% and 46%, respectively (15). Due to these promising data, we focused on the anti-PD-1/anti-CTLA-4 combination therapy.

To validate the relevance of extracranial disease in the context of anti-PD-1/anti-CTLA-4 therapy for BrM, we compared therapeutic efficacy between mice bearing intracranial tumors only (representing a conventional intracranial tumor transplantation model (17, 27)), and mice bearing tumors at both sites. Strikingly, in the absence of extracranial disease, the anti-PD-1/anti-CTLA-4 combination failed to extend the survival or to reduce the intracranial tumor burden (**Fig. 1F-H,**

Supplemental Fig. 1D-E). This observation reproduced in a B16 model overexpressing an immunogenic ovalbumin (OVA) xenoantigen (28), hence demonstrating that increasing the inherent immunogenicity of the model is not sufficient to induce anti-tumor responses in the brain following PD-1/CTLA-4 blockade (**Fig. 1I**). The requirement of extracranial disease for intracranial anti-PD-1/anti-CTLA-4 efficacy was further confirmed in the Ret melanoma model (19, 29), demonstrating that our findings are model-independent (**Fig. 1J**; see **Supplemental Fig. 1F-H** for the establishment of experimental timeline in Ret model). Taken together, our results reveal that the intracranial activity of anti-PD-1/anti-CTLA-4 depends on the extracranial tumor, highlighting the importance of including the clinically-relevant extracranial disease in this context.

Immune response in the brain is enhanced in the presence of extracranial disease

To evaluate the immunological response in the brain upon anti-PD-1/anti-CTLA-4 therapy and the role of extracranial disease, we analyzed the tumor-infiltrating immune cells in intracranial B16 tumors by flow cytometry (**Supplemental Fig. 2A**). Although anti-PD-1/anti-CTLA-4 therapy resulted in a small increase in intra-tumoral CD45⁺ cells in the absence of extracranial disease, a major anti-PD-1/anti-CTLA-4-induced increase in this cell population, and significant expansion of CD3⁺ T cells, were observed only in the presence of s.c. tumor (**Fig. 2A, B, C, Supplemental Fig. 2B**). Likewise, anti-PD-1/anti-CTLA-4-induced increases in CD8⁺ T cells (**Fig. 2D**), CD11b⁺F4/80⁺CD45^{high} (25, 30, 31) bone marrow-derived macrophages (**Fig. 2G**), and CD11b⁺F4/80⁺CD45^{low} (25, 30, 31) brain-resident microglia (**Fig. 2H**) were detected only in the presence of extracranial disease. In contrast, the percentages of total CD4⁺ T cells, FoxP3⁺CD4⁺ regulatory T cells (T_{reg}) and FoxP3⁺CD4⁺ effector T cells (T_{eff}) increased upon anti-PD-1/anti-CTLA-4 treatment independent of extracranial tumor (**Fig. 2D**). The CD4⁺T_{eff} / T_{reg} ratio, the increase of which was previously associated with therapeutic efficacy in some studies (32), remained unaltered (**Fig. 2E**). The proportion of NK cells also remained unchanged (**Fig. 2F**). Importantly, similar changes in immune cell populations within intracranial tumors were observed in the Ret melanoma model (**Supplemental Fig. 3A**).

To determine whether monotherapies are sufficient to induce infiltration of immune cells into intracranial tumors, we analyzed immune cell populations in mice bearing intracranial and extracranial B16 tumors, following anti-PD-1 or anti-CTLA-4 monotherapy. Both monotherapies

failed to increase the proportion of immune cells in intracranial tumors as compared to IgG-treated mice (**Supplemental Fig. 3B**). Thus, the lack of therapeutic efficacy observed for the two monotherapies was in line with their failure to induce immune cell infiltration into intracranial tumors.

To evaluate the immunological response in the brain at the molecular level, intracranial B16 tumors were profiled using next generation RNA sequencing (mRNAseq). Differential gene expression analysis (adjusted p value < 0.05) indicated that the presence of extracranial disease did not cause any significant alterations in gene expression levels in IgG-treated control mice (**Fig. 3A**). In contrast, the presence of extracranial disease resulted in altered expression of 4154 genes in anti-PD-1/anti-CTLA-4-treated mice. This suggested that extracranial disease has significant impact on the intracranial tumor only in the context of PD-1/CTLA-4 blockade. In contrast, anti-PD-1/anti-CTLA-4 therapy itself had impact on gene expression both in the absence (906 differentially expressed genes) and presence (621 differentially expressed genes) of extracranial disease. Importantly, brain tumors from mice with intracranial and extracranial tumors undergoing anti-PD-1/anti-CTLA-4 treatment had significantly distinct transcriptomes as compared to the other 3 experimental groups (**Fig. 3B**). Gene ontology (GO) enrichment analysis identified classes of genes significantly altered upon anti-PD-1/anti-CTLA-4 therapy in the presence of extracranial disease, revealing significant upregulation in GO terms relating to NK cell activation and chemotaxis (**Fig. 3C**), T cell activation (**Fig. 3D, Supplemental Fig. 4A**), and microglia/macrophage activation and migration (**Fig. 2E, Supplemental Fig. 4B**).

Hence, our data revealed that anti-PD-1/anti-CTLA-4 efficacy in the brain correlates with intra-tumoral increase in CD8⁺ T cells, macrophages and microglia, as well as upregulation of genes involved in activation of T cells, NK cells, and microglia/macrophages. This implies that anti-PD-1/anti-CTLA-4 activity relies on multiple immune cell populations, the activation and/or intra-tumoral increase of which were dependent on the presence of extracranial tumor.

CD8⁺ T cells and NK cells are required for the intracranial efficacy of anti-PD-1/anti-CTLA-4 therapy

The upregulation of T cell and NK cell activation markers in association with the intracranial anti-PD-1/anti-CTLA-4 efficacy prompted us to investigate the functional role of these cell populations

in the context of PD-1/CTLA-4 blockade. Antibody-mediated depletion of NK cells, CD4⁺ or CD8⁺ T cells was performed in mice bearing intracranial and extracranial B16 tumors undergoing anti-PD-1/anti-CTLA-4 therapy (**Fig. 4A**). Efficient depletion of respective cell populations in the blood and tumor tissue was confirmed by flow cytometry (**Supplemental Fig. 5**). While the depletion of CD4⁺ T cells had no impact on survival (**Fig. 4B**), depletion of either NK (**Fig. 4C**) or CD8⁺ T cells (**Fig. 4D**) resulted in a significant loss of survival advantage observed upon anti-PD-1/anti-CTLA-4 therapy, demonstrating a critical involvement of these cell populations.

To further characterize T cells in intracranial B16 tumors, we analyzed the expression of known T cell activation/exhaustion markers (e.g. CD25, CD69, Granzyme B, Eomesodermin (EOMES), T-cell immunoglobulin and mucin domain containing-3 (TIM3)) in CD4⁺ and CD8⁺ T cells by flow cytometry (**Supplemental Fig. 6A**). We detected no changes in the percentages of cells expressing the investigated markers or in their protein expression levels (mean fluorescence intensity; MFI) (**Supplemental Fig. 6B, C**). Therefore, marked increase in the overall gene expression levels of T cell activation markers following anti-PD-1/anti-CTLA-4 therapy in the presence of extracranial tumor (**Fig. 3D**) can be explained by the increased intra-tumoral percentage of CD8⁺ T cells (**Fig. 2D**). Our findings thus imply that inhibition of intracranial tumor growth was caused by an increase in CD8⁺ T cell numbers rather than their enhanced intra-tumoral activation.

Anti-PD-1/anti-CTLA-4 treatment enhances trafficking of CD8⁺ T cells to intracranial tumors

We next sought to determine the underlying mechanism for the increase in intra-tumoral CD8⁺ T cells following anti-PD-1/anti-CTLA-4 therapy. The proportion of proliferative CD8⁺ T cells within intracranial B16 tumors was high (~75% Ki67⁺ cells) and remained unaffected by anti-PD-1/anti-CTLA-4 treatment or the presence of extracranial disease (**Fig. 5A**). This finding excluded intra-tumoral expansion of CD8⁺ T cells as a major driver of their intra-tumoral increase. We therefore reasoned that enhanced recruitment of CD8⁺ T cells from outside the brain is likely responsible for their accumulation in intracranial tumors following PD-1/CTLA-4 blockade. To investigate this, we analyzed the trafficking of CD8⁺ T cells to intracranial tumors by performing an adoptive transfer of CellTrace Violet (CTV)-labeled CD8⁺ T cells (4×10^6) in mice with

extracranial plus intracranial tumors. T cell donor and recipient mice both received 2 doses of anti-PD-1/anti-CTLA-4 or IgG (**Fig. 5B**), which was sufficient to significantly increase the overall percentage of intra-tumoral CD8⁺ T cells in treated as compared to control mice (**Supplemental Fig. 8A**). CD8⁺ T cells from IgG-treated donor mice were transferred into IgG-treated recipient mice, and cells from anti-PD-1/anti-CTLA-4-treated donor mice were transferred into anti-PD-1/anti-CTLA-4-treated recipient mice (**Fig. 5B**). Analysis of intra-tumoral CTV⁺ CD8⁺ T cells at 18 hours post-adoptive transfer demonstrated a strong increase (~14-fold) in CD8⁺ T cell homing to intracranial tumors in the presence of anti-PD-1/anti-CTLA-4 therapy (**Fig. 5C, D**). Notably, we observed no significant proliferation of adoptively transferred T cells within 18 hours, and therefore increase in intra-tumoral CTV⁺ CD8⁺ T cells was attributable exclusively to their trafficking and not their proliferation (**Supplemental Fig. 8B**).

To investigate whether systemic T cell expansion may contribute to enhanced accumulation of CD8⁺ T cells in intracranial B16 tumors, we analyzed peripheral T cell populations in the blood and spleens. All anti-PD-1/anti-CTLA-4-dependent changes in ratios of peripheral CD8⁺ T cells, CD4⁺ T_{eff} and T_{reg} cells occurred independently of extracranial disease (**Supplemental Fig. 7A, B**). In contrast, PD-1/CTLA-4 blockade-induced increase in CD44⁺CD62L⁻ effector CD8⁺ T cells in blood was significantly enhanced in the presence of extracranial disease, and thus correlated with the intracranial anti-PD-1/anti-CTLA-4 efficacy (**Fig. 5E**). Analysis of intracranial tumors revealed that the majority of intra-tumoral CD8⁺ T cells were CD44⁺CD62L⁻ effector cells in both treated and control mice (**Fig. 5F**). This prompted us to compare homing of CD44⁺CD62L⁻ effector and CD44⁻CD62L⁺ naïve CD8⁺ T cells to intracranial tumors. Notably, the percentage of CD8⁺ T cells within pooled spleen and lymph nodes was slightly higher in anti-PD-1/anti-CTLA-4 treated mice (10.3%) as compared to the IgG treated mice (9%) (**Fig. 5G, top**). Moreover, the percentage of CD44⁺CD62L⁻ cells within CD8⁺ T cell population was higher in anti-PD-1/anti-CTLA-4 treated mice (3.8%) as compared to IgG treated mice (2.2%) (**Fig. 5G, bottom**). Thus, to ensure that the same numbers of cells per investigated CD8⁺ T cell population are used for adoptive transfer in the control and therapy group, we sorted CD44⁺CD62L⁻ and CD44⁻CD62L⁺ CD8⁺ T cell populations from pooled spleens and lymph nodes of IgG- and anti-PD-1/anti-CTLA-4-treated mice, respectively. CTV-labeled CD44⁺CD62L⁻ (1×10^5) and CD44⁻CD62L⁺ (2.4×10^6) cells, respectively, were transferred into recipient mice that received the corresponding treatment (**Fig. 5D**). Analysis of CTV⁺ CD8⁺ T cells within intracranial tumors at 18 hours post-transfer

confirmed that only CD44⁺CD62L⁻ cells efficiently homed to intracranial tumors (**Fig. 5H**). Notably, we detected a tendency towards more efficient homing of CD44⁺CD62L⁻ CD8⁺ T cells isolated from anti-PD-1/anti-CTLA-4-treated mice (0.009±0.004% all cells) as compared to the IgG control mice (0.006±0.002% all cells; **Fig. 5I**). In summary, this suggested that an enhanced homing of CD8⁺ T cells to intracranial tumors following anti-PD-1/anti-CTLA-4 therapy is mainly due to the peripheral expansion of CD44⁺CD62L⁻ effector cells. However, a tendency towards more efficient homing of effector CD8⁺ T cells isolated from anti-PD-1/anti-CTLA-4-treated mice as compared to IgG-treated mice implied that additional factors may be involved.

PD-1/CTLA-4 blockade upregulates T cell trafficking determinants on tumor blood vessels

Consistent with a tendency towards increased trafficking of CD8⁺ effector T cells to intracranial tumors following anti-PD-1/anti-CTLA-4 treatment, KEGG pathway analysis identified “Leukocyte transendothelial migration” as one of the pathways significantly upregulated in intracranial tumors following PD-1/CTLA-4 blockade in the presence of extracranial disease as compared to the other 3 experimental groups (**Fig. 6A**). Among the upregulated genes, Vascular cell adhesion molecule 1 (VCAM-1) and Intercellular adhesion molecule 1 (ICAM-1) - two major endothelial T cell entry receptors (33) - were upregulated 6.4- and 3.8-fold, respectively (**Fig. 6A**). VCAM-1 expression on tumor blood vessels was confirmed by immunofluorescence (**Fig. 6B**). Analysis of VCAM-1 and ICAM-1 expression on tumor endothelial cells by flow cytometry confirmed a significant upregulation of both receptors following anti-PD-1/anti-CTLA-4 therapy in the presence of extracranial disease (**Fig. 6C, D, Supplemental Fig. 8C**). The percentage of ICAM-1⁺ endothelial cells increased from ~75 to 90% and the percentage of VCAM-1⁺ endothelial cells from ~5 to 45%. Moreover, the expression levels of both receptors were ~3-fold elevated, as indicated by a significant increase in MFI (**Fig. 6D**).

Following anti-PD-1/anti-CTLA-4 therapy, blood vessels within the tumor-adjacent brain parenchyma remained negative for VCAM-1 expression (**Supplemental Fig. 8D**), indicating that the upregulation of T cell entry receptors was restricted to the tumor microenvironment. In line with this finding, gene expression levels of IFN γ – a known inducer of endothelial VCAM-1 and ICAM-1 (33) – were upregulated within intracranial tumors following anti-PD-1/anti-CTLA-4 therapy in mice bearing tumors at both sites (**Supplemental Fig. 8E**). Concurrently, intracellular

flow cytometry staining revealed a significant increase in the percentage of IFN γ ⁺ cells within NK cell and macrophage populations (**Fig. 6E, top**), while TNF α expression remained unaltered (**Supplemental Fig. 8F**). Although such an increase in IFN γ expression was not detected for CD8⁺ T cells and microglia, their increased proportion within intracranial tumors per se also contributed towards an overall increase in IFN γ (**Fig. 6E, bottom**).

In summary, our data indicate that anti-PD-1/anti-CTLA-4 treatment – in the context of clinically relevant extracranial disease – increases intra-tumoral CD8⁺ T cells in the brain through peripheral expansion of CD44⁺CD62L⁻ effector CD8⁺ T cells and potentiation of their trafficking to intracranial tumors, the latter potentially occurring via upregulation of T cell entry receptors ICAM1/VCAM1 on the tumor vasculature.

Discussion

In this study we reveal that extracranial disease plays a critical role for the intracranial efficacy of combined anti-PD-1 plus anti-CTLA-4 therapy. This was demonstrated through analysis of intracranial tumor-dependent survival, quantification of tumor growth, characterization of tumor-infiltrating immune cell populations, and gene expression analysis (mRNAseq). Importantly, clinically observed intracranial activity of anti-PD-1/anti-CTLA-4 therapy (4, 5, 11-15) could be recapitulated only in the tumor transplantation model with intracranial plus extracranial tumor, but not in the model bearing only intracranial cancer lesions, which is a conventional brain tumor transplantation model (17, 27). Moreover, superior intracranial activity of anti-PD-1/anti-CTLA-4 combination therapy in our optimized model was in line with the reported higher intracranial response rates with combined anti-PD-1 plus anti-CTLA-4 (50%) than anti-PD-1 alone (21%) in drug-treatment naïve patients (15). Thus, by including extracranial tumor, we achieved an important improvement in simulating human disease and clinical responses to PD-1 and CTLA-4 blockade in the brain, and thus our model is expected to significantly advance preclinical studies on immunotherapy in BrM.

In terms of adaptive immune responses, the brain is markedly different from other major sites of metastasis, such as the skin, lungs and bones (26). While antigens from these other sites are efficiently transported to the peripheral lymphoid organs where T cell priming/activation occurs, a body of literature shows that antigens located within the brain are less accessible and transported to lymph nodes at a different location (e.g. cervical lymph nodes), and/or presented in a different way (20-23). In line with this notion, our study reveals that successful targeting of melanoma BrM with anti-PD-1/anti-CTLA-4 antibodies relies on: (i) tumor antigens present at extracranial locations and (ii) release of CD8⁺ T cells from immune checkpoint inhibition and their activation occurring outside the brain. Notably, release of T cells from immune checkpoint inhibition and their subsequent increased proliferation following anti-CTLA-4 and anti-PD-1 therapy is mainly observed within secondary lymphoid organs and within the tumor microenvironment, respectively (14). Accordingly, increase in proliferation of intra-tumoral CD8⁺ T cells occurs in s.c. B16 melanoma tumors following PD-1 blockade alone or in combination with anti-CTLA-4 or radiotherapy (34-36). However, in contrast to extracranial sites, the blood-brain barrier limits access of therapeutic antibodies into brain tumors, which may preclude anti-PD-1-induced release of T cells from proliferation block once they have entered the brain tumor microenvironment.

Indeed, in our study, anti-PD-1/anti-CTLA-4 combination failed to increase the proportion of proliferative CD8⁺ T cells and their expression of activation markers within intracranial tumors. This provides strong evidence that the release of CD8⁺ T cells from immune checkpoint inhibition occurred mainly outside the brain, and that intracranial anti-PD-1/anti-CTLA-4 activity relies on the subsequent recruitment of these extracranially activated CD8⁺ T cells to intracranial tumors.

Our data suggest that enhanced CD8⁺ T cell trafficking to intracranial tumors following anti-PD-1/anti-CTLA-4 therapy in the context of extracranial disease may be enhanced through the upregulation of VCAM-1 and ICAM-1 on tumor blood vessels. IFN γ was identified as one of the potential factors involved in the upregulation of these vascular receptors. NK cells and microglia/macrophages were the main source of anti-PD-1/anti-CTLA-4-induced IFN γ upregulation. This finding may explain why intracranial anti-PD-1/anti-CTLA-4 efficacy required NK cells and correlated with intra-tumoral increase in macrophages. Notably, the latter may have been recruited to intracranial tumors through colony stimulating factor 1 (CSF-1), a potent microglia/macrophages chemoattractant (37) which, in our study, was found to be upregulated 2.8-fold following anti-PD-1/anti-CTLA-4 therapy in the presence of extracranial tumor. Several studies reported IFN γ increase in tumors following ICI treatment, although this has not yet been connected to the upregulation of vascular T cell homing determinants or enhanced T cell trafficking (34, 36, 38). Nevertheless, IFN γ -dependent upregulation of ICAM-1 on choroid plexus epithelial cells in the brain has been recently shown to increase T cell infiltration into the brain in models of spinal cord injury and Alzheimer's disease (39, 40).

More than half of patients with metastatic melanoma develop BrM and, with ICI becoming the frontline therapy for metastatic disease, it is critical to understand how immune checkpoint inhibition can be optimized in the brain. Since the intracranial anti-PD-1/anti-CTLA-4 efficacy seemed to rely on the recruitment of activated CD8⁺ T cells from outside the brain, strategies aimed at enhancing T cell homing - for example through adoptive T cell therapy using T cells with enhanced BrM-homing characteristics - have a strong potential to improve the efficacy of ICI in the brain. Moreover, our findings on the critical role of extracranial disease for intracranial anti-PD-1/anti-CTLA-4 efficacy are of relevance to the optimization of ICI for primary non-metastatic brain cancers, in particular glioma. Notably, in contrast to clinical evidence for anti-PD-1 activity in melanoma BrM (12, 13), a recent phase III clinical trial of nivolumab in glioma was negative (<https://news.bms.com/press-release/bmy/bristol-myers-squibb-announces-results-checkmate->

[143-phase-3-study-opdivo-nivoluma](#)). Our data suggest that the combination of ICI with strategies that boost the peripheral antigen-specific T cell activation, such as cancer vaccines, may also improve anti-PD-1/anti-CTLA-4 efficacy in metastatic and non-metastatic brain cancers.

Materials and Methods

In vivo model of brain metastases

All procedures were approved by the University of Leeds Animal Welfare & Ethical Review Committee and performed under the approved UK Home Office project license in line with the Animal (Scientific Procedures) Act 1986 and in accordance with the UK National Cancer Research Institute Guidelines for the welfare of animals (41).

Six to eight weeks old female C57Bl/6J or B6N-Tyrc-Brd/BrdCrCl (B6 Albino) mice were purchased from Charles River Laboratories, UK. B16 F1, B16/OVA or Ret melanoma cells (please refer to Supplementary methods for cell line details) were injected s.c. on the flank to generate extracranial tumors (2×10^5 B16 and B16/OVA cells; 1×10^5 Ret cells). To generate intracranial tumors, cancer cells (1×10^5 B16/Fluc and B16/OVA/Fluc cells; 1×10^3 Ret/Fluc cells) were stereotactically injected into the striatum (2 mm right from the midline, 2 mm anterior from bregma, 3 mm deep). Prior to treatment, mice used in experiments with B16 and B16/OVA models were randomized into groups based on the intracranial bioluminescence signals ensuring equal distribution of tumor burden across groups. Mice used in experiments with the Ret melanoma model were randomized into groups so as to ensure an equal proportion of mice from different litters per group (randomization based on the bioluminescence signal intensity was not possible at early time points due to the low number of implanted cells in this model). Anti-PD-1 (RMP1-14), anti-CTLA-4 (9D9) and IgG control (MPC11) purchased from Bio-X-Cell were administered i.p. at 200 μ g per mouse as indicated.

Experimental group sizes were determined with power analysis (power = 80%, significance level = 5%, difference to be detected between groups = 50%) using the mean values and standard deviations from our pilot studies. All animals were included in the survival analysis and tumor growth analysis. In cases where tumors were too small to obtain sufficient material for facs analysis, the animals were excluded from this analysis. All outliers were included in the analysis. The study was not blinded.

Quantification of extracranial tumor growth was performed by caliper measurement. Quantification of intracranial tumor growth was performed via non-invasive bioluminescence imaging using IVIS Spectrum and Living Image software (PerkinElmer).

Immune cell depletion was achieved through i.p. administration of anti-CD8 α (YTS.4; Bio-X-Cell), anti-CD4 (GK1.5; Bio-X-Cell), or anti-asialo-GM1 that depletes NK cells (polyclonal rabbit IgG; Cedarlane) at 100 μ g per mouse every 4 days. For detection of IFN γ and TNF α by flow cytometry, mice received 250 μ g Brefeldin A (Sigma) i.v. 6 hours prior to tissue harvesting. Adoptive T cell transfer experiments are described under Supplementary methods.

Immunofluorescence

Immunofluorescence was performed as previously described (25). Details are provided under Supplementary methods.

Flow cytometry

Mice were perfused with saline. Tumors were mechanically disrupted and enzymatically dissociated (25). The blood (collected from tail vein) and splenocytes were treated with ammonium-chloride-potassium buffer to lyse red blood cells. Samples were blocked with 10% rat serum and FcR blocking reagent (Miltenyi) prior to surface antigen staining. FoxP3/Transcription Factor Staining Buffer Set (eBioscience) was used for intracellular staining of nuclear antigens following manufacturer's instructions. Intracellular fixation buffer and Permeabilization buffer (eBioscience) were used for staining of cytoplasmic antigens following manufacturer's instructions. Cells were analyzed on BD LSRII Flow Cytometry Analyzer (Life Technologies). Data were quantified using FACSDiva software. The gates were set based on appropriate isotype controls. Antibody details are provided in Supplementary methods.

RNAseq and gene expression analysis

Details are provided under Supplementary methods.

Statistical analysis

Statistical analysis was carried out using Graph Pad Prism v7 (Graph Pad Software). Statistical tests used were analysis of variance (ANOVA) with a post hoc test for multiple comparisons

(Tukey's multiple comparisons test), Mann-Whitney test and Mann-Whitney U Test, as specified in figure legends. All tests except the Mann-Whitney U Test were 2-tailed statistical tests. Statistical significance in survival experiments was determined with Log-rank test. Error bars represent standard error of the mean (SE), except in Fig. 6E where the bars represent standard deviations. The number of biological replicates for each experiment is stated in figure legends. Each experiment was performed 2-4 times, as specified. Data from repeat experiments were combined as indicated in figure legends.

Data availability statement

Gene expression data (mRNAseq) will be deposited in an approved database prior to publication.

Acknowledgments: We thank Dr. Neta Erez (Tel Aviv University) for donating Ret melanoma cells and Prof. Richard Vile (Mayo Clinic) for donating B16/OVA cells. We thank Prof. Georgina V. Long and Dr. Alexander M. Menzies (Melanoma Institute Australia, The University of Sydney and Royal North Shore and Mater Hospitals, Sydney, New South Wales, Australia) for important discussions on clinical studies and help with the presentation and citation of clinical data. We thank Dr. Heiko Wurdak (University of Leeds) for critical reading and input to the manuscript. We would like to thank staff working at St. James's Biological Services for their continuous support with in vivo work, Adam Davison and Elizabeth Straszynski for their support with flow cytometry, Gary Shaw and Samantha Turnbull for supporting the experimental work.

Author contributions: ML, AM, RJS, EJI and DT designed research. DT, TA, KJS, JW, NR, RJB and ML performed research. ML wrote the paper. RJS and AM had a significant input to the manuscript.

Financial support: This work was supported by the Yorkshire Cancer Research grant awarded to ML and AM, and by a Cancer Research UK grant awarded to AM. TA was supported by The Brain Tumour Charity, JW was supported by the Brain Tumour Research and Support across Yorkshire (grant to ML), NR was supported by a Marie Curie Career Integration grant awarded to ML, and KJS was funded by the Experimental Cancer Medicine Centres Network.

References:

1. Davies MA, et al. (2011) Prognostic factors for survival in melanoma patients with brain metastases. *Cancer* 117(8):1687-1696.
2. Long GV & Margolin KA (2013) Multidisciplinary approach to brain metastasis from melanoma: the emerging role of systemic therapies. *Am Soc Clin Oncol Educ Book*:393-398.
3. Sampson JH, Carter JH, Jr., Friedman AH, & Seigler HF (1998) Demographics, prognosis, and therapy in 702 patients with brain metastases from malignant melanoma. *J Neurosurg* 88(1):11-20.
4. Ajithkumar T, Parkinson C, Fife K, Corrie P, & Jefferies S (2015) Evolving treatment options for melanoma brain metastases. *Lancet Oncol* 16(13):e486-497.
5. Igor Puzanov JDW, Paolo A Ascierto, Omid Hamid, Kim Margolin (2013) Anti-CTLA-4 and BRAF Inhibition in patients with metastatic melanoma and brain metastases. *Expert Reviews Dermatology* 8(5):479-487.
6. Kamphorst AO & Ahmed R (2013) Manipulating the PD-1 pathway to improve immunity. *Curr Opin Immunol* 25(3):381-388.
7. Walker LS & Sansom DM (2011) The emerging role of CTLA4 as a cell-extrinsic regulator of T cell responses. *Nat Rev Immunol* 11(12):852-863.
8. Larkin J, et al. (2015) Combined Nivolumab and Ipilimumab or Monotherapy in Untreated Melanoma. *New Engl J Med* 373(1):23-34.
9. Boutros C, et al. (2016) Safety profiles of anti-CTLA-4 and anti-PD-1 antibodies alone and in combination. *Nat Rev Clin Oncol* 13(8):473-486.
10. Berghoff AS, Venur VA, Preusser M, & Ahluwalia MS (2016) Immune Checkpoint Inhibitors in Brain Metastases: From Biology to Treatment. *Am Soc Clin Oncol Educ Book*

- 35:e116-122.
11. Margolin K, et al. (2012) Ipilimumab in patients with melanoma and brain metastases: an open-label, phase 2 trial. *Lancet Oncol* 13(5):459-465.
 12. Goldberg SB, et al. (2016) Pembrolizumab for patients with melanoma or non-small-cell lung cancer and untreated brain metastases: early analysis of a non-randomised, open-label, phase 2 trial. *Lancet Oncol* 17(7):976-983.
 13. Gonzalez-Cao M, et al. (2017) Pembrolizumab for advanced melanoma: experience from the Spanish Expanded Access Program. *Clin Transl Oncol*.
 14. Parakh S, et al. (2017) Efficacy of anti-PD-1 therapy in patients with melanoma brain metastases. *Br J Cancer* 116(12):1558-1563.
 15. Long GV, et al. (2017) A randomized phase II study of nivolumab or nivolumab combined with ipilimumab in patients (pts) with melanoma brain metastases (mets): The Anti-PD1 Brain Collaboration (ABC). *Journal of clinical oncology* 35:suppl; abstr 9508.
 16. H. Tawbi, PF, A. Algazi, O. Hamid, F. S. Hodi, S. Moschos, N. Khushalani, R. Gonzalez, C. Lao, M. Postow, M. B. Atkins, M. Ernstoff, I. Puzanov, R. Kudchadkar, R. Thomas, A. Tarhini, J. Jiang, A. Avila, S. Demelo, K. Margolin (2017) Efficacy and Safety of Nivolumab Plus Ipilimumab in Patients with Melanoma Metastatic to the Brain: Results of the Phase II Study CheckMate 204. *Journal of clinical oncology* 35, suppl; abstr 9507 (2017).
 17. Cohen JV, et al. (2016) Melanoma central nervous system metastases: current approaches, challenges, and opportunities. *Pigment Cell Melanoma Res* 29(6):627-642.
 18. Cho JH, et al. (2015) AKT1 Activation Promotes Development of Melanoma Metastases. *Cell Rep* 13(5):898-905.

19. Schwartz H, et al. (2016) Incipient Melanoma Brain Metastases Instigate Astrogliosis and Neuroinflammation. *Cancer Res* 76(15):4359-4371.
20. Binder DC, Davis AA, & Wainwright DA (2016) Immunotherapy for cancer in the central nervous system: Current and future directions. *Oncoimmunology* 5(2):e1082027.
21. Carson MJ, Doose JM, Melchior B, Schmid CD, & Ploix CC (2006) CNS immune privilege: hiding in plain sight. *Immunol Rev* 213:48-65.
22. Ransohoff RM & Engelhardt B (2012) The anatomical and cellular basis of immune surveillance in the central nervous system. *Nat Rev Immunol* 12(9):623-635.
23. Harling-Berg CJ, Park TJ, & Knopf PM (1999) Role of the cervical lymphatics in the Th2-type hierarchy of CNS immune regulation. *J Neuroimmunol* 101(2):111-127.
24. Alonso-Camino V, et al. (2014) The profile of tumor antigens which can be targeted by immunotherapy depends upon the tumor's anatomical site. *Mol Ther* 22(11):1936-1948.
25. Rippaus N, et al. (2016) Metastatic site-specific polarization of macrophages in intracranial breast cancer metastases. *Oncotarget* 7(27):41473-41487.
26. Tas F (2012) Metastatic behavior in melanoma: timing, pattern, survival, and influencing factors. *J Oncol* 2012:647684.
27. Damsky WE, Theodosakis N, & Bosenberg M (2014) Melanoma metastasis: new concepts and evolving paradigms. *Oncogene* 33(19):2413-2422.
28. Merrick A, et al. (2008) Autologous versus allogeneic peptide-pulsed dendritic cells for anti-tumour vaccination: expression of allogeneic MHC supports activation of antigen specific T cells, but impairs early naive cytotoxic priming and anti-tumour therapy. *Cancer Immunol Immunother* 57(6):897-906.
29. Zhao F, et al. (2009) Activation of p38 mitogen-activated protein kinase drives dendritic

- cells to become tolerogenic in ret transgenic mice spontaneously developing melanoma. *Clin Cancer Res* 15(13):4382-4390.
30. Ford AL, Goodsall AL, Hickey WF, & Sedgwick JD (1995) Normal adult ramified microglia separated from other central nervous system macrophages by flow cytometric sorting. Phenotypic differences defined and direct ex vivo antigen presentation to myelin basic protein-reactive CD4+ T cells compared. *J Immunol* 154(9):4309-4321.
 31. Hickman SE, et al. (2013) The microglial sensome revealed by direct RNA sequencing. *Nature neuroscience* 16(12):1896-1905.
 32. Simpson TR, et al. (2013) Fc-dependent depletion of tumor-infiltrating regulatory T cells co-defines the efficacy of anti-CTLA-4 therapy against melanoma. *J Exp Med* 210(9):1695-1710.
 33. Prendergast CT & Anderton SM (2009) Immune cell entry to central nervous system--current understanding and prospective therapeutic targets. *Endocr Metab Immune Disord Drug Targets* 9(4):315-327.
 34. Peng W, et al. (2012) PD-1 blockade enhances T-cell migration to tumors by elevating IFN-gamma inducible chemokines. *Cancer Res* 72(20):5209-5218.
 35. Spranger S, et al. (2014) Mechanism of tumor rejection with doublets of CTLA-4, PD-1/PD-L1, or IDO blockade involves restored IL-2 production and proliferation of CD8(+) T cells directly within the tumor microenvironment. *J Immunother Cancer* 2:3.
 36. Twyman-Saint Victor C, et al. (2015) Radiation and dual checkpoint blockade activate non-redundant immune mechanisms in cancer. *Nature* 520(7547):373-377.
 37. Coniglio SJ, et al. (2012) Microglial stimulation of glioblastoma invasion involves epidermal growth factor receptor (EGFR) and colony stimulating factor 1 receptor (CSF-

- 1R) signaling. *Mol Med* 18:519-527.
38. Das R, et al. (2015) Combination therapy with anti-CTLA-4 and anti-PD-1 leads to distinct immunologic changes in vivo. *J Immunol* 194(3):950-959.
 39. Baruch K, et al. (2016) PD-1 immune checkpoint blockade reduces pathology and improves memory in mouse models of Alzheimer's disease. *Nat Med* 22(2):135-137.
 40. Kunis G, et al. (2013) IFN-gamma-dependent activation of the brain's choroid plexus for CNS immune surveillance and repair. *Brain* 136(Pt 11):3427-3440.
 41. Workman P, et al. (2010) Guidelines for the welfare and use of animals in cancer research. *Br J Cancer* 102(11):1555-1577.
 42. Trapnell C, et al. (2010) Transcript assembly and quantification by RNA-Seq reveals unannotated transcripts and isoform switching during cell differentiation. *Nat Biotechnol* 28(5):511-515.

Figure legends

Fig. 1. Inhibition of intracranial tumor growth and prolonged survival following anti-PD-1/CTLA-4 therapy require the presence of extracranial disease. (A) Survival of C57Bl/6J mice following intracranial implantation of B16/Fluc melanoma cells (n=8) and time to the establishment of extracranial B16 s.c. tumors with a diameter of 15 mm (n=10). (B) Experimental time line for the implantation of cancer cells in B16 model and therapeutic schedule. (C) Survival of mice with intracranial (B16/Fluc) plus extracranial (B16) tumors following the administration of anti-PD-1, anti-CTLA-4, anti-PD-1/CTLA-4, or IgG control (n=8). The overall significance is shown. Individual p values are given in Fig. S1C. (D) Quantification of intracranial B16/Fluc tumor burden via bioluminescence imaging (n=20/24). Fold change in bioluminescence signal intensity between days 12 and 5 (e.g. pre/post-treatment) for mice treated with anti-PD-1/CTLA-4 or IgG. (E) Quantification of extracranial B16 tumor burden on day 12 via caliper measurement (n=20/24). (F) Survival following anti-PD-1/anti-CTLA-4 or IgG administration was compared between mice bearing only intracranial B16/Fluc tumors and mice bearing intracranial B16/Fluc and extracranial B16 tumors. The overall significance is indicated. Individual p values are summarized in Fig. S1D. (G) Representative images of intracranial bioluminescence signals (B16/Fluc tumors). (H, I) Fold change in intracranial bioluminescence signal intensity between days 12 and 5 (e.g. pre/post-treatment) for the B16/Fluc (H) and B16/OVA/Fluc (I) melanoma models (n=21/21/20/24 for B16/Fluc; n=16/16/15/25 for B16/OVA/Fluc). Labeling as in F. (J) Quantification of intracranial Ret/Fluc melanoma burden (n=8/8/8/13). Bioluminescence signal intensity (total flux; photons/second) is shown. Labeling as in F. Significant differences in C and F were determined with Log-rank test. Significant differences in D, E, H, I and J were determined with Mann-Whitney test (* p \leq 0.05; ** p \leq 0.01; *** p \leq 0.001). Data from 2 (I) or 3 (C-F, H) independent experiments are shown.

Fig. 2. Analysis of immune cell populations in intracranial B16 tumors reveals extracranial tumor- and PD-1/CTLA-4 blockade-dependent changes. (A) Representative dot plots of CD45⁺ cell population. (B) Representative immunofluorescence images of CD45⁺ cells infiltrating intracranial tumors. (C) Percentages of CD45⁺ hematopoietic cells and CD3⁺ T cells as quantified by flow cytometry. Significant p values are summarized in Fig. S2B. (D-H) Analysis

of different T cell subpopulations (D), CD4⁺ T_{eff} / T_{reg} ratio (E), NK cells (F), CD11b+F4/80+CD45^{high} macrophages (G) and CD11b+F4/80+CD45^{low} microglia (H) within intracranial tumors by flow cytometry. Labeling as in D. All analyses were performed on day 12. Combined data from 3 independent experiments are shown (n=10/13/16/24 per group for CD45+, NK, microglia and macrophages; n=14/16/17/22 per group for T cell subpopulations). Significant differences were determined by ANOVA with a post hoc test (* p≤0.05; ** p≤0.01; *** p≤0.001; **** p≤0.0001). Detailed ANOVA parameters are provided in the Supplemental Table 1.

Fig. 3. PD-1/CTLA-4 blockade- and extracranial disease-dependent molecular changes within intracranial B16 tumors. (A) Number of genes differentially expressed within intracranial tumors between experimental groups. (B) Unsupervised hierarchical clustering and heat map of top 2000 differentially expressed genes. (C-E) Unsupervised hierarchical clustering and heat maps of differentially expressed genes involved in NK cell function (C; the list of genes is based on the significantly enriched GO terms displayed on the left), T cell function (D; example genes are shown; heat map including all genes is given in Fig. S4B), and microglia (E). The analysis was performed on day 12.

Fig. 4. CD8⁺ T cells and NK cells are required for intracranial efficacy of PD-1/CTLA-4 blockade in B16 model. (A) Experimental timeline indicating administration of respective immune cell-depleting antibodies. (B-D) Survival analysis of anti-PD-1/anti-CTLA-4-treated mice bearing intracranial and extracranial tumors following in vivo depletion of CD4⁺ T cells, CD8⁺ T cells, or NK cells, respectively (n=16; pooled data from 2 independent experiments). Significant differences were determined with Log-rank test. P values shown are for comparison between the anti-PD-1/CTLA-4 group and the respective group in which a specific immune cell population has been depleted.

Fig. 5. Anti-PD-1/anti-CTLA4 therapy in the context of extracranial disease potentiates trafficking of CD8⁺ T cells to intracranial B16 tumors. (A) Analysis of Ki67⁺ CD8⁺ T cells within intracranial tumors by flow cytometry. (B) Schematic representation of adoptive transfer experiments using CellTrace Violet (CTV)-labelled CD8⁺ T cells. (C) Representative dot plot of

adoptively transferred CTV+ CD8+ T cells detected within intracranial tumors. **(D)** Analysis of adoptively transferred CTV+ CD8+ T cells in intracranial tumors at 18 hours post-transfer (n=10). Labeling as in A. **(E, F)** Analysis of CD44+CD62L- CD8+ effector T cells in blood (E) and intracranial tumors (F) on day 12 (n=6/6/7/12 for blood; n=10/10 for intracranial tumors). Labeling as in A. **(G)** Dot plots of pooled spleen and lymph node cells isolated from donor mice for use in adoptive CD8+ T cell transfer experiments. Percentages of total CD8+ T cells and CD44+CD62L- cells within the CD8+ T cell population are indicated. **(H)** Representative dot plots of adoptively transferred CTV-tagged CD44+CD62L- (top) and CD44-CD62L+ (bottom) CD8+ T cells detected within intracranial tumors at 18 hours post-transfer. **(I)** Analysis of adoptively transferred CTV-tagged CD44+CD62L- CD8+ T cells in intracranial tumors at 18 hours post-transfer (n=5). Significant differences in A and E were determined by ANOVA with a post hoc test, and in D, F and I with a two-tailed T-test (unequal variance); ** $p \leq 0.01$; **** $p \leq 0.0001$. Data from at least 2 repeat experiments were pooled for analysis (A-F). Detailed ANOVA and T-test parameters are provided in Supplemental Table 1.

Fig. 6. PD-1/CTLA-4 blockade upregulates vascular T cell trafficking determinants in intracranial B16 tumors. **(A)** Unsupervised hierarchical clustering and heat map of genes differentially expressed within the “Leukocyte transendothelial migration” KEGG pathway. FC: fold change; pval: p value. **(B)** Immunofluorescence staining for CD31 (endothelial cells) and VCAM-1 within intracranial tumors from treated mice bearing intracranial and extracranial tumors. **(C)** Representative dot plots of endothelial cells (CD45-CD31+) and ICAM-1 / VCAM-1 staining within the endothelial cell population. **(D)** Analysis of ICAM-1 and VCAM-1 expression in intracranial tumors by flow cytometry (n=5/5/7/9). One out of two representative experiments is shown. **(E)** Analysis of intracellular IFN γ staining in intracranial tumors isolated from Brefeldin A-treated mice (n=7). Percentage of IFN γ + cells within respective immune cell populations (top) and within total cell population (bottom) is shown. Data from two independent experiments were pooled for analysis. Significant differences in D and E-bottom were determined by ANOVA with a post hoc test, and in E-top with Mann-Whitney U Test (one-tailed, $p \leq 0.05$); *** $p \leq 0.001$; **** $p \leq 0.0001$. Detailed ANOVA parameters are provided in Supplemental Table 1.

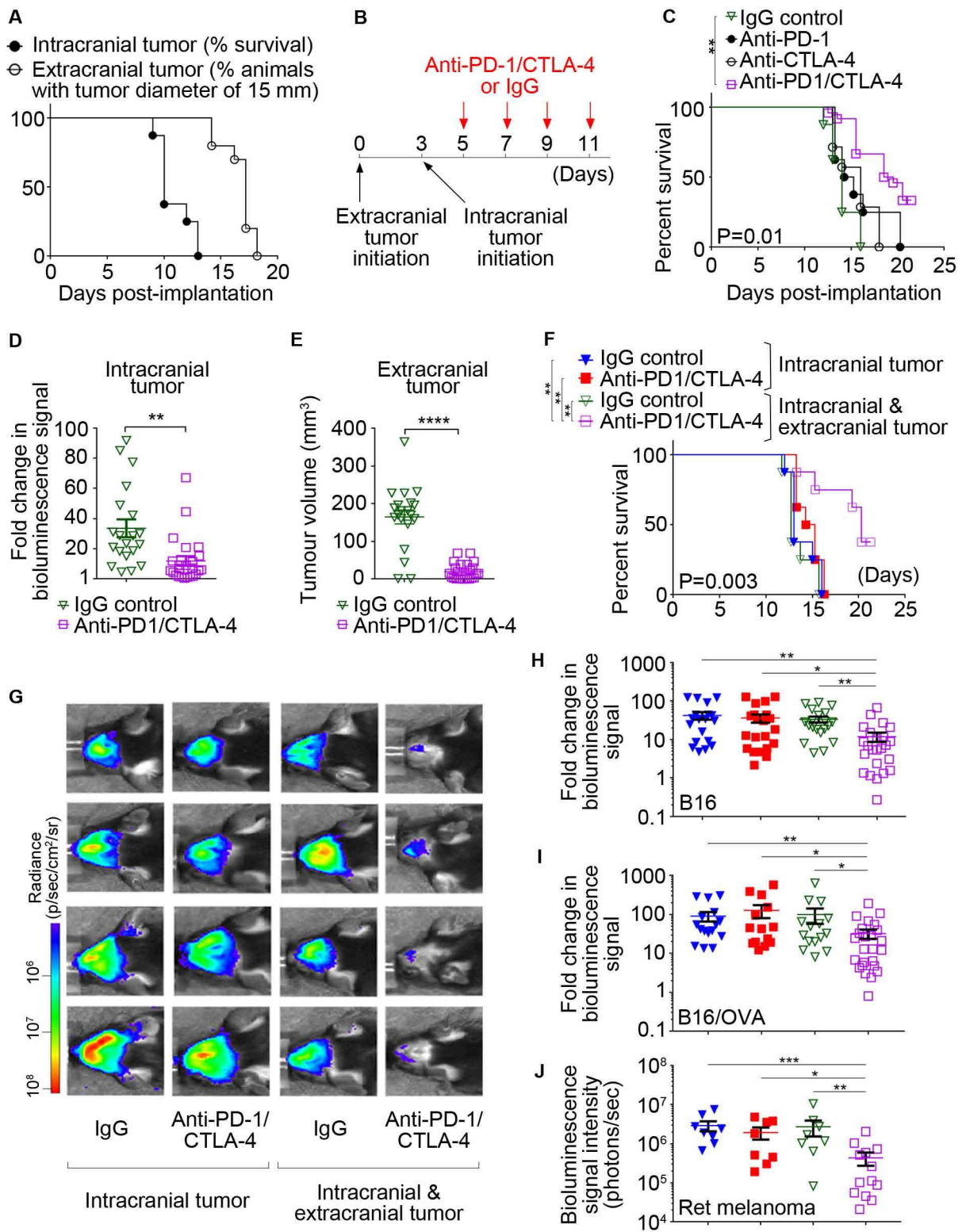


Fig. 1

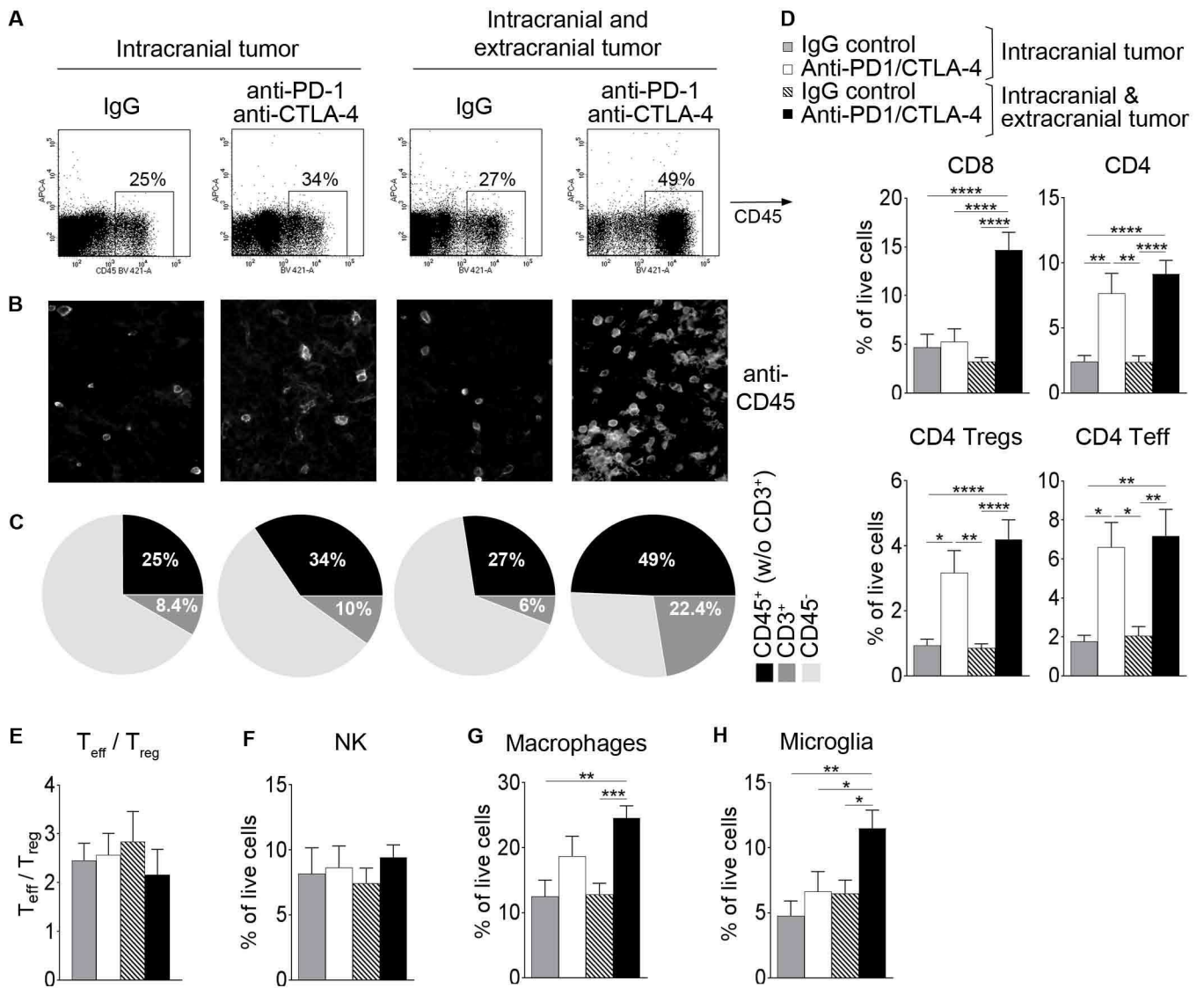
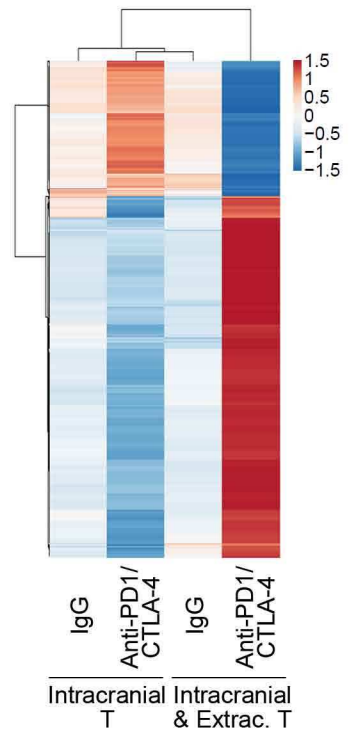


Fig. 2

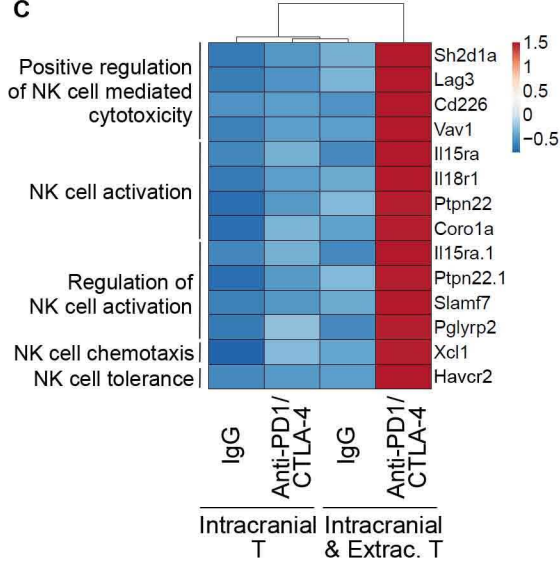
A

Group 1	Group 2	Nm. DEG
Intracranial T - IgG	Intracranial & Extrac. T - IgG	0
Intracranial T - anti-PD1/CTLA-4	Intracranial & Extrac. T - anti-PD-1/CTLA-4	4154
Intracranial T - IgG	Intracranial T - anti-PD1/CTLA-4	906
Intracranial & Extrac. T - IgG	Intracranial & Extrac. T - anti-PD-1/CTLA-4	621

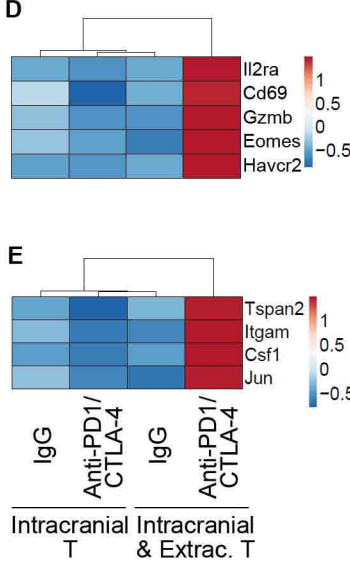
B



C



D



E

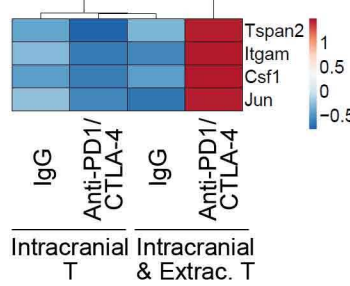


Fig. 3

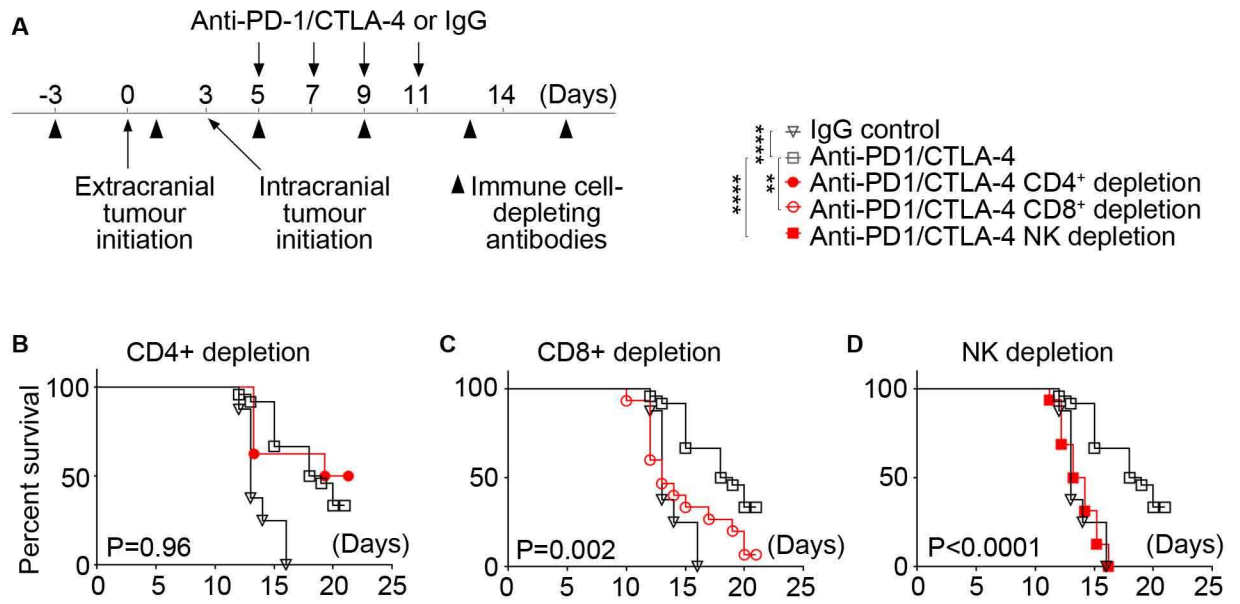


Fig. 4

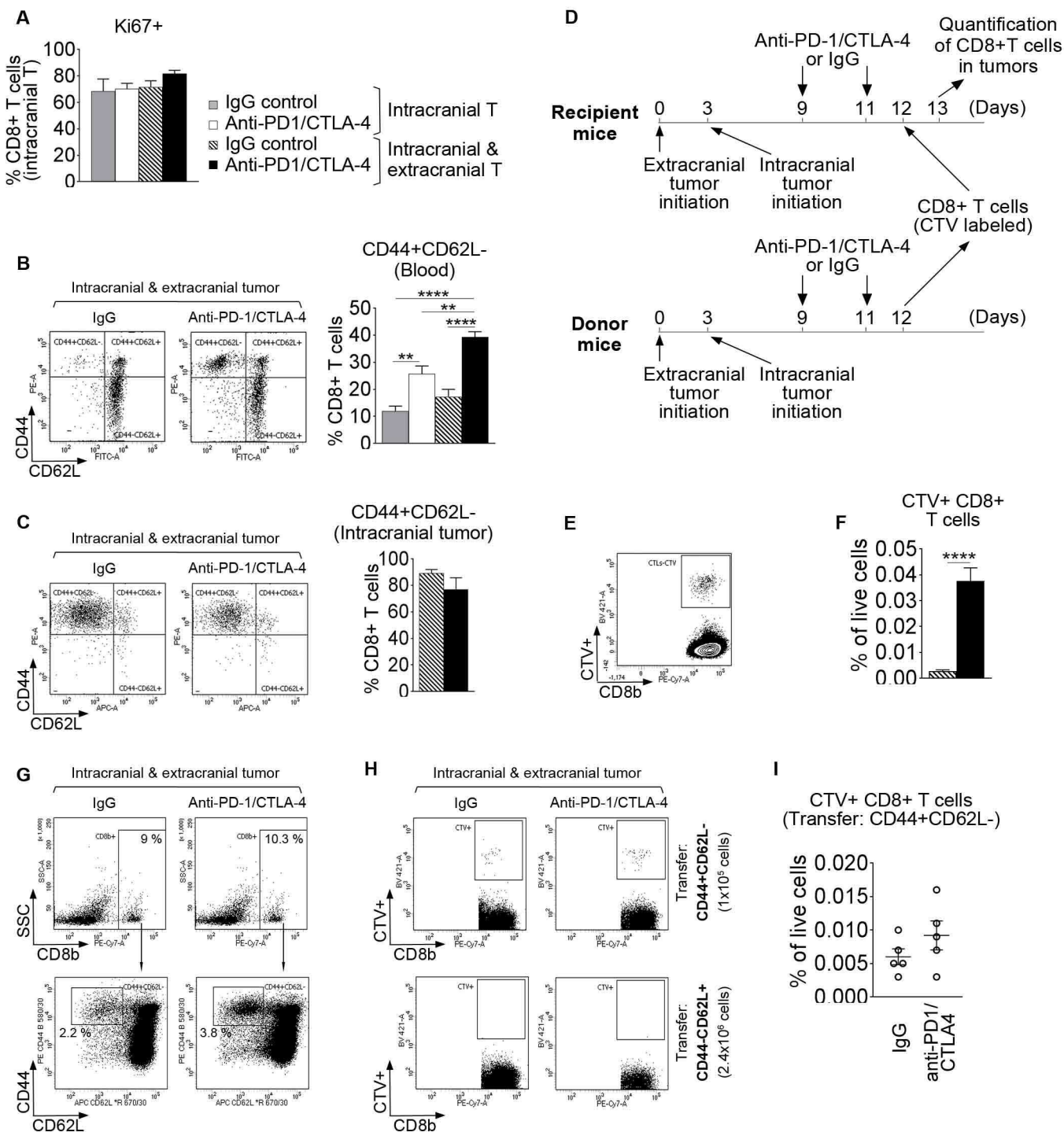
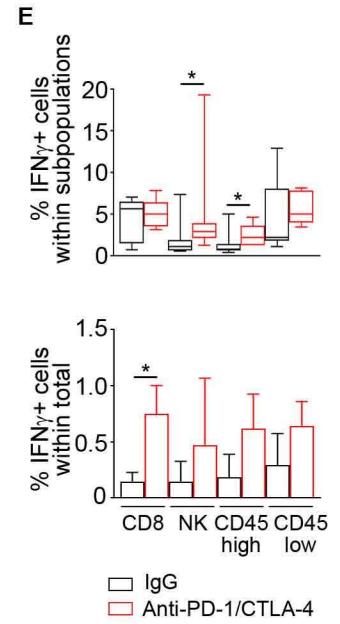
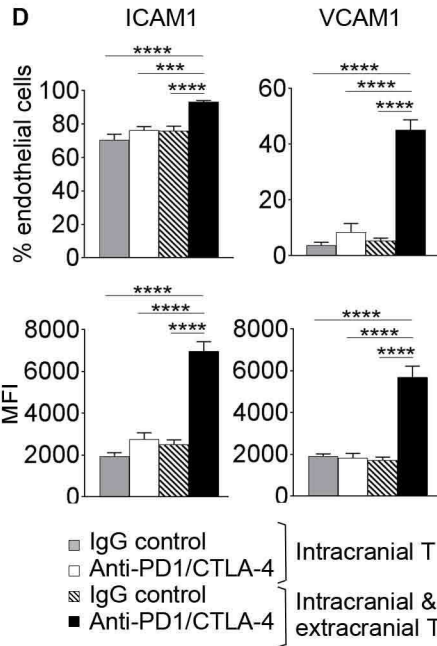
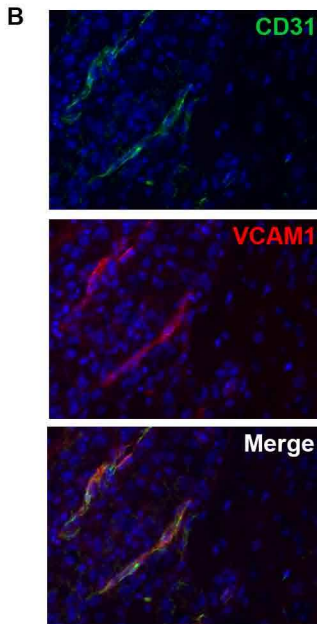
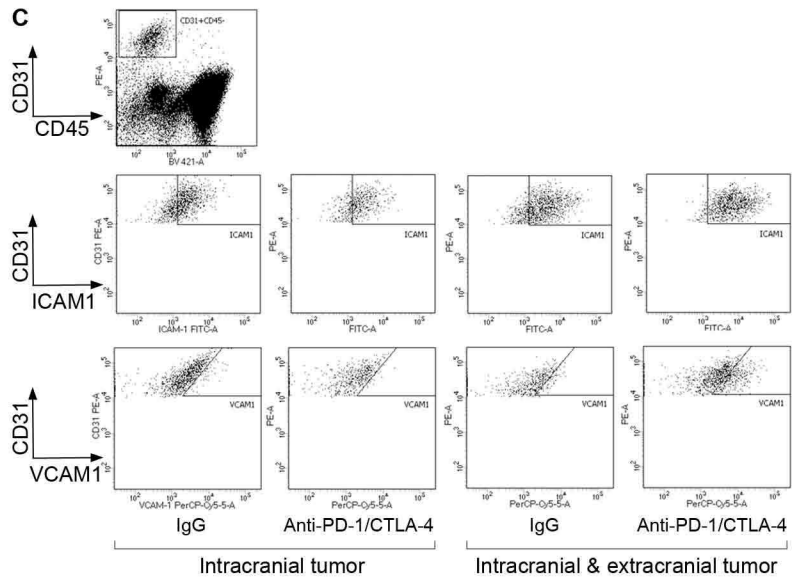
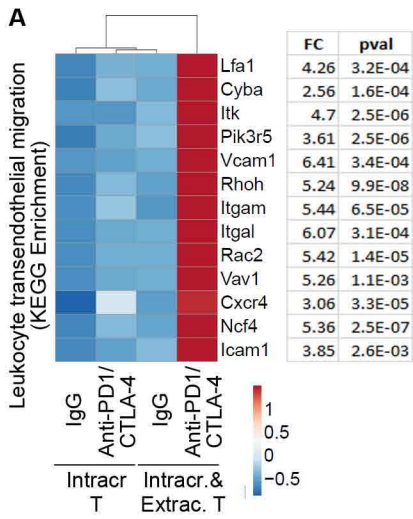


Fig. 5



Supplemental methods

Cell lines

B16 F1 melanoma cells were obtained from the American Type Culture Collection (ATCC) and used between P4 and P8. B16/OVA cells were a kind gift from Prof. R. Vile, Mayo Clinic. OVA expression by this cell line was confirmed by qPCR. Ret melanoma cells (19, 29) were kindly provided by Dr. Neta Erez, Tel Aviv University. Mycoplasma test was performed routinely upon receipt of the cells and then every 6 months. All cell lines were tested for the presence of murine pathogens by IDEXX BioResearch (IMPACT IV PCR profile) and confirmed to be pathogen-free. B16 and B16/OVA cells were cultured in Dulbecco's modified eagle medium (DMEM) (Sigma-Aldrich) supplemented with 10% fetal bovine serum (FBS) (Gibco), 1x L-glutamine (Gibco) and 1x penicillin streptomycin (Pen strep) (Gibco). Ret melanoma cells were cultured in RPMI-1640 medium (Sigma-Aldrich) supplemented with 10% fetal bovine serum (FBS) (Gibco), 1x L-glutamine (Gibco), 1x sodium pyruvate (Gibco) and 1x penicillin streptomycin (Gibco). For some experiments, cancer cells were stably transduced with Firefly luciferase-expressing lentiviral vector (25).

Flow cytometry: antibody details

Anti-CD3 (17A2), anti-CD8 (53-6.7), anti-CD8b (YTS156.7.7), anti-CD4 (GK1.5), anti-FoxP3 (3G3), anti-CD49b (DX5), anti-Eomes (REA116), anti-CD69 (H1.2F3), anti-CD25 (7D4), and anti-MHCII (M5/114.15.2) were from Miltenyi. Anti-CD45 (30F11), anti-CD8b (53-5.8), anti-NKp46 (29A1.4), anti-CD11b (M1/70), anti-NK1.1 (PK136), anti-IFN γ (XMG1.2), anti-CD44 (IM7), anti-CD62L (MEL-14), and anti-VCAM-1 (429 (MVCAM.A)) were from Biolegend. Anti-

Granzyme B (NGZB), anti-Ki67 (SolA15), anti-TIM-3 (RMT3-23), anti- TNF α (MP6-XT22), anti-CD31 (390), and anti-ICAM1 (YN1/1.7.4) were from eBioscience. Anti-F4/80 was from AbD Serotec.

Immunofluorescence

Immunofluorescence was performed as previously described (25). Mice were perfused with saline and the isolated tissue was fixed in 4% paraformaldehyde for 24 hours. The tissue was cut into 10 μ m frozen sections on slides. Following blocking with goat serum in 0.03% Triton-X-100 / PBS, the sections were stained with anti-VCAM1 (clone MVCAM.A; Biolegend) and anti-CD31 (rabbit polyclonal; Abcam) antibody overnight, followed by fluorophore-conjugated secondary antibodies. Images were acquired with AxioImager Z1 fluorescence microscope equipped with AxioCam MRc5 digital camera using AxioVision Rel. 4.7 software (Zeiss).

Adoptive transfer of CD8⁺ T cells

Donor mice received two doses of anti-PD-1/CTLA-4 therapy or IgG, respectively, as specified. Cells from inguinal, axial, and mesenteric lymph nodes, and the splenocytes, were pooled and CD8⁺ T cells were isolated using CD8⁺ T cell isolation kit (Miltenyi). CD8⁺ T cells were labelled with CellTrace Violet (Thermo Fisher Scientific) following manufacturer's instructions and 4×10^6 cells were injected i.v. into recipient mice. The latter also received two doses of anti-PD-1/CTLA-4 therapy or IgG, respectively, prior to adoptive T cell transfer, as specified under results. Tissue was analyzed by flow cytometry 18 hours post-adoptive transfer.

For adoptive transfer of CD44⁺CD62L⁻ and CD44⁻CD62L⁺ CD8⁺ T cell populations, total CD8⁺ T cells were isolated and labeled with CTV as described above, and subsequently stained with anti-CD8b, anti-CD44, and anti-CD62L antibodies. CD44⁺CD62L⁻ and CD44⁻CD62L⁺ populations were isolated via FACS using BD INFLUX cell sorter (BD Biosciences) and injected i.v. into recipient mice (treated as described above). We injected 1×10^5 CD44⁺CD62L⁻ cells and 2.4×10^6 CD44⁻CD62L⁺ cells per mouse.

Isolation of RNA, generation of sequencing libraries, and mRNAseq

Mice were perfused with saline. RNA from fresh tumor tissue (biological triplicates) was isolated using RNeasy Total RNA Isolation kit (Qiagen). Generation of sequencing libraries, mRNA sequencing and data analysis were performed by Novogene. A total amount of 3 µg RNA per sample was used as input material for RNA sample preparations. Sequencing libraries were generated using NEBNext® Ultra™ RNA Library Prep Kit for Illumina® (NEB, USA) following manufacturer's recommendations and index codes were added to attribute sequences to each sample. Briefly, mRNA was purified from total RNA using poly-T oligo-attached magnetic beads. Fragmentation was carried out using divalent cations under elevated temperature in NEBNext First Strand Synthesis Reaction Buffer (5x). First strand cDNA was synthesized using random hexamer primer and M-MuLV Reverse Transcriptase (RNase H). Second strand cDNA synthesis was subsequently performed using DNA Polymerase I and RNase H. Remaining overhangs were converted into blunt ends via exonuclease/polymerase activities. After adenylation of 3' ends of DNA fragments, NEBNext Adaptor with hairpin loop structure were ligated to prepare for hybridization. In order to select cDNA fragments of preferentially 150~200 bp in length, the library fragments were purified with AMPure XP system (Beckman Coulter, Beverly, USA). USER

Enzyme (NEB, USA) was used with size-selected, adaptor-ligated cDNA at 37°C for 15 min followed by 5 min at 95 °C before PCR. PCR was performed with Phusion High-Fidelity DNA polymerase, Universal PCR primers and Index (X) Primer. PCR products were purified (AMPure XP system) and library quality was assessed on the Agilent Bioanalyzer 2100 system.

The clustering of the index-coded samples was performed on a cBot Cluster Generation System using TruSeq PE Cluster Kit v3-cBot-HS (Illumina) according to the manufacturer's instructions. After cluster generation, the library preparations were sequenced on an Illumina HiSeq platform and 125 bp/150 bp paired-end reads were generated.

Sequencing data analysis

Data analysis was performed by Novogene. Quality control raw data (raw reads) in fastq format were firstly processed through in-house perl scripts. Clean data (clean reads) were obtained by removing reads containing adapter, reads containing poly-N and low quality reads from raw data. At the same time, Q20, Q30 and GC content of the clean data were calculated. All the downstream analyses were based on the clean data with high quality.

To perform reads mapping to the reference genome, the reference genome and gene model annotation files were downloaded from the genome website directly. Index of the reference genome was built using Bowtie v2.2.3 and paired-end clean reads were aligned to the reference genome using TopHat v2.0.12.

HTSeq v0.6.1 was used to count the reads numbers mapped to each gene (Quantification of gene expression level). FPKM of each gene was calculated based on the length of the gene and reads count mapped to this gene. FPKM, expected number of Fragments Per Kilobase of transcript

sequence per Million base pairs sequenced, considers the effect of sequencing depth and gene length for the reads count at the same time, and is currently the most commonly used method for estimating gene expression levels (42).

Differential gene expression analysis

Differential expression analysis of two conditions/groups was performed using the DESeq R package (1.18.0). The resulting P-values were adjusted using the Benjamini and Hochberg's approach for controlling the false discovery rate. Genes with an adjusted P-value found by DESeq were assigned as differentially expressed.

GO and KEGG enrichment analysis of differentially expressed genes

Gene Ontology (GO) enrichment analysis of differentially expressed genes was implemented by the GOrse R package, in which gene length bias was corrected. GO terms with corrected P-value less than 0.05 were considered significantly enriched by differential expressed genes. We used KOBAS software to test the statistical enrichment of differential expression genes in KEGG pathways (<http://www.genome.jp/kegg/>).

Supplementary figure legends:

Supplemental Figure 1. B16 melanoma tumor growth. (A) Growth curve of B16 melanoma s.c. tumors (n=8). (B) Growth curve of Firefly luciferase (Fluc)-tagged B16 melanoma intracranial tumors (B16/Fluc) as quantified by bioluminescence imaging (n=8). Fold change in bioluminescence signal intensity between the respective day and day 2 is shown (C) Statistical

significance (p values) for the survival experiment shown in Fig. 1C. **(D)** Statistical significance (p values) for the survival experiment shown in Fig. 1F. **(E)** Representative images of B16/Fluc tumor-bearing brains. **(F)** Growth curve of Ret melanoma s.c. tumors (n=5). **(G)** Survival curves for mice bearing intracranial Ret/Fluc melanoma tumors following implantation of 1×10^3 , 1×10^4 and 1×10^5 cells, respectively (n=5). **(H)** Experimental time line for the implantation of cancer cells s.c. (Ret; 1×10^5) and intracranially (Ret/Fluc; 1×10^3), and the therapeutic schedule. The time line was determined based on s.c. and intracranial tumor growth shown in F and G.

Supplemental Figure 2. Analysis of immune cell populations in intracranial B16/Fluc tumors by flow cytometry. **(A)** Gating strategy and representative contour plots for analysis of different immune cell populations. **(B)** Statistical significance (p values) for pair-wise comparison of percentages of CD45⁺ and CD3⁺ cells between experimental groups as determined by ANOVA with a post hoc test (***) $p \leq 0.001$; **** $p \leq 0.0001$).

Supplemental Figure 3. Quantification of immune cell populations within intracranial tumors. **(A)** Percentages of different immune cell populations within intracranial Ret/Fluc melanoma tumors following combined PD-1/CTLA-4 blockade or IgG treatment, as quantified by flow cytometry (n=7/5/6/7). **(B)** Percentages of different immune cell populations within intracranial B16/Fluc melanoma tumors following anti-PD-1 and anti-CTLA-4 monotherapies in comparison to IgG treatment, as quantified by flow cytometry (n=7). Significant differences were determined by ANOVA with a post hoc test (* $p \leq 0.05$; ** $p \leq 0.01$; *** $p \leq 0.001$).

Supplemental Figure 4. Gene expression analysis (mRNAseq) of intracranial B16 tumors.

(A) Unsupervised hierarchical clustering and heat map of differentially expressed genes involved in T cell function. (B) Unsupervised hierarchical clustering and heat map of differentially expressed genes related to macrophage function.

Supplemental Figure 5. Depletion of specific immune cell populations in B16 model in vivo.

Efficient depletion of CD4⁺ T cells, CD8⁺ T cells and NK cells, respectively, was confirmed in the blood (A) and within intracranial tumors (B) by flow cytometry.

Supplemental Figure 6. Quantification of T cell activation/exhaustion markers in B16 model by flow cytometry. (A) Gating strategy and representative contour plots for analysis of different activation markers in CD8⁺ T cells by flow cytometry. (B) Quantification of marker expression in CD8⁺ T cells within intracranial tumors was performed by flow cytometry. Combined data from 3 independent experiments are shown for CD25 and CD69 (n=13/16/17/22). Combined data from 2 independent experiments are shown for all other markers (n=7/11/11/11). (C) Quantification of CD25 and CD69 expression in CD4⁺ T cells within intracranial tumors was performed by flow cytometry. Combined data from 3 independent experiments are shown (n=13/16/17/22). Significant differences in B and C were determined by ANOVA with a post hoc test.

Supplemental Figure 7. Quantification of T cells in B16 model in the periphery. (A) Total number of cells and percentages of different T cell subpopulations in spleens were quantified by flow cytometry. Combined data from 2 independent experiments are shown (n=14/13/17/26). (B) Percentages of different T cell subpopulations in the blood were quantified by flow cytometry. Combined data from 2 independent experiments are shown (n=14/13/17/26). Significant

differences were determined by ANOVA with a post hoc test (* $p \leq 0.05$; ** $p \leq 0.01$; *** $p \leq 0.001$; **** $p \leq 0.0001$).

Supplemental Figure 8. Adoptive transfer of CD8⁺ T cells and upregulation of T cell homing determinants within B16 tumor microenvironment. (A) Percentages of CD8⁺ T cells within intracranial tumors were quantified by flow cytometry following 2 doses of anti-PD-1/anti-CTLA-4 or IgG treatment (n=5). (B) Histograms of adoptively transferred CTV⁺ CD8⁺ T cells in the spleen and intracranial tumors at 18 hours post-transfer. (C) Quantification of ICAM-1⁺ and VCAM-1⁺ endothelial cells within intracranial tumors at an early time point following 2 doses of anti-PD-1/anti-CTLA-4 or IgG treatment (n=4). (D) Immunofluorescence staining for CD31 (endothelial cells) and VCAM-1 within intracranial tumors in the experimental group receiving anti-PD-1/CTLA-4 treatment in the presence of extracranial disease. Tumor region (left) and adjacent brain parenchyma (right) are separated by a dotted line. Tumor blood vessels are positive for VCAM-1 staining (red arrows), while normal brain vessels show no VCAM-1 expression (white arrows). (E) Quantification of IFN γ expression within intracranial tumors by mRNAseq using biological triplicates. Fpkms: Fragments Per Kilobase of transcript sequence per Millions base pairs sequenced. (F) Quantification of TNF α expression within intracranial tumor-infiltrating immune cells by intracellular flow cytometry. Significant differences in A and D were determined by ANOVA with a post hoc test (* $p \leq 0.05$; ** $p \leq 0.01$).

Supplemental Table 1. Top: ANOVA parameters. F value, degrees of freedom (DF), and p values are shown for the data that have been analyzed by ANOVA. The figure number for each data set is specified in the first column. **Bottom:** T-test parameters. T-value, degrees of freedom

(DF), and p value are shown for the data that have been analyzed by T-test. The figure number for each data set is specified in the first column.

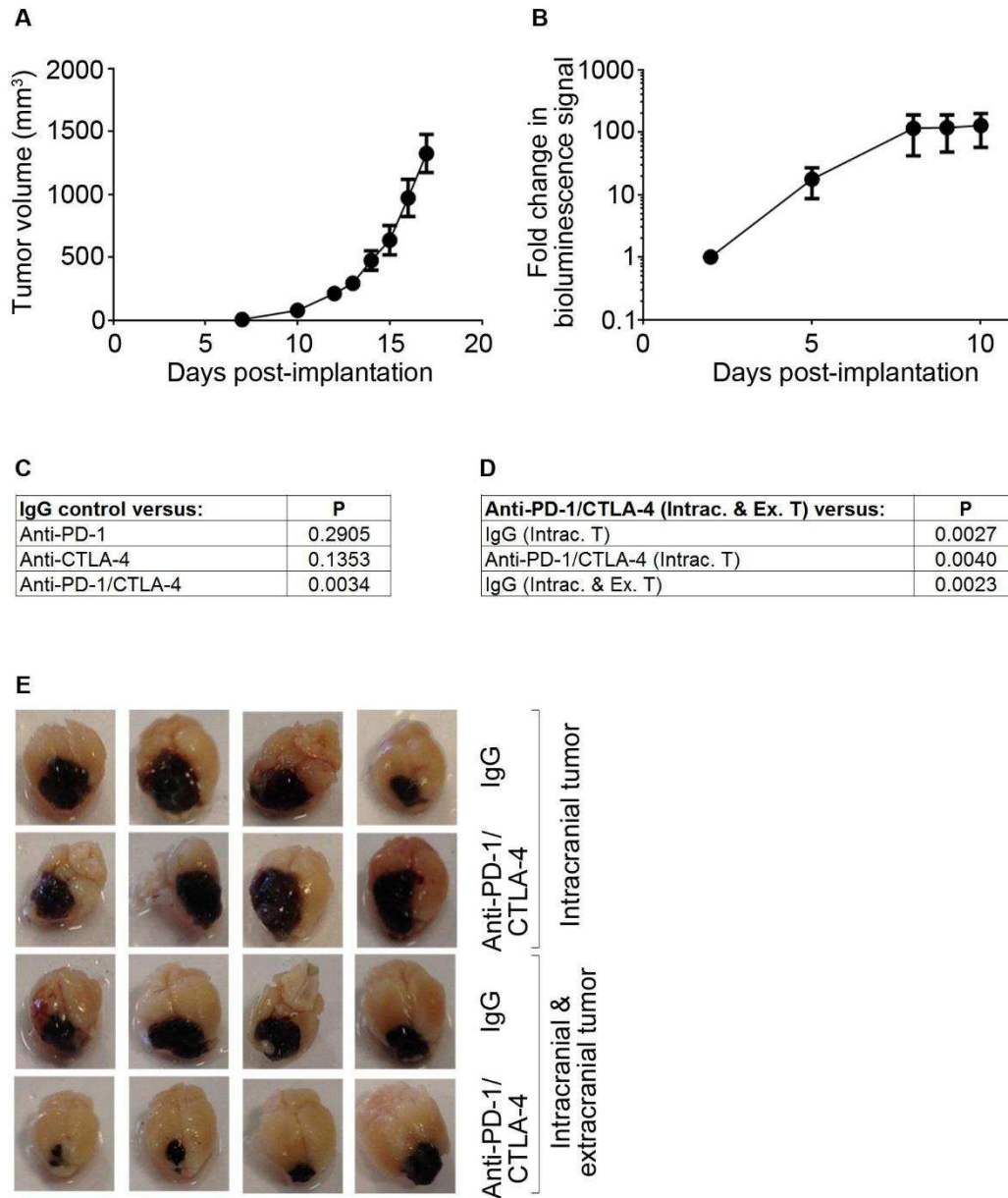


Figure S1

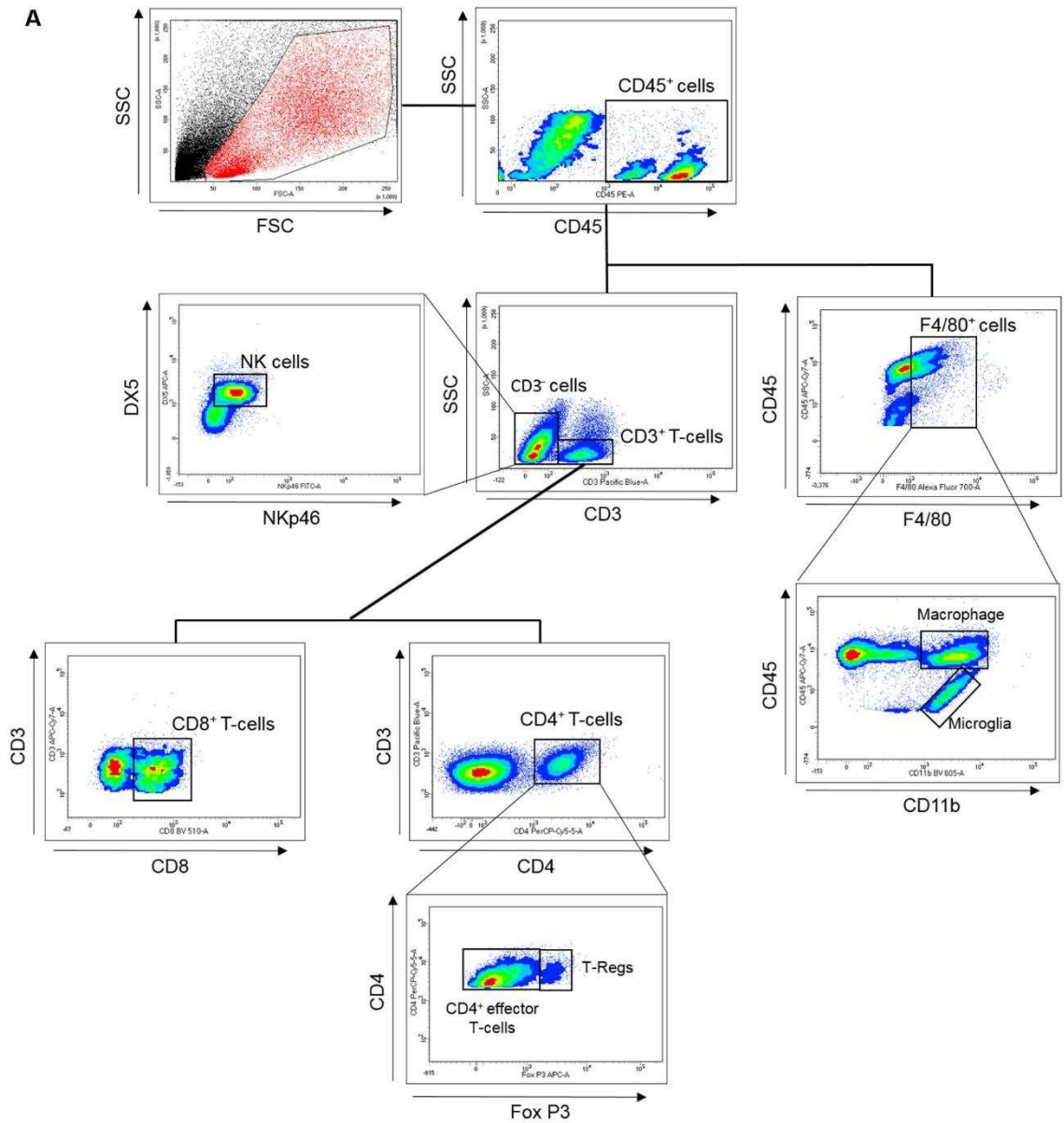


Figure S2

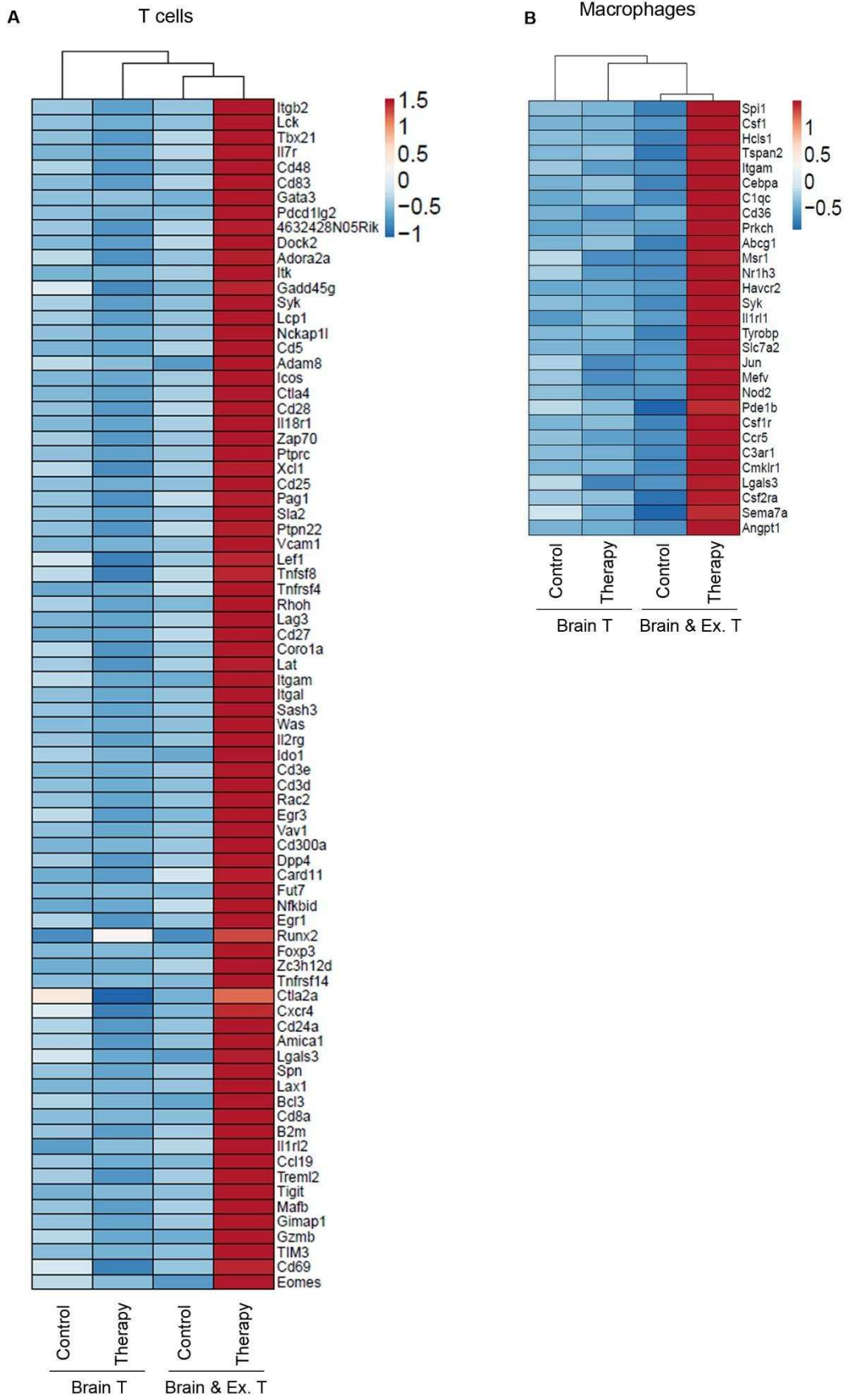
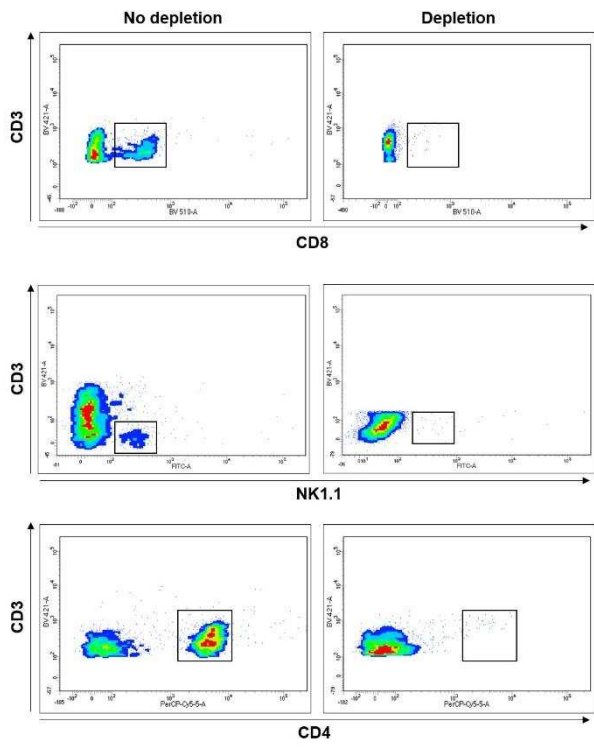
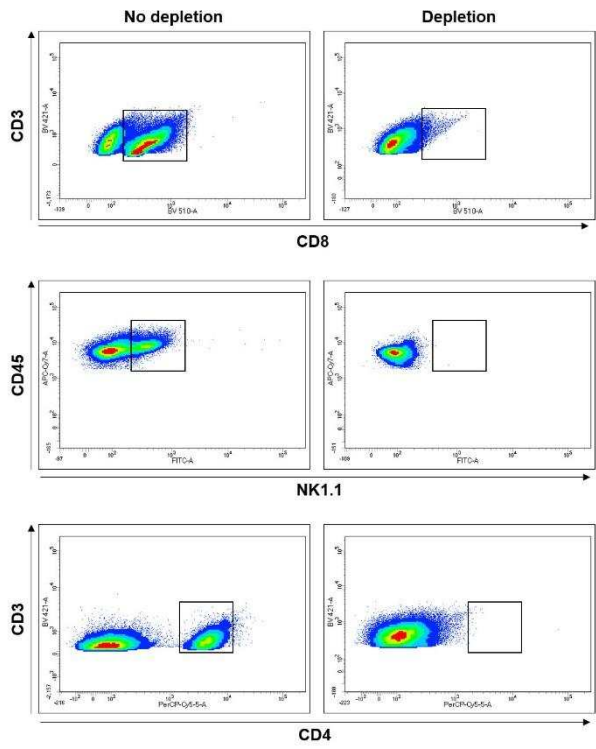


Figure S3

A**B****Figure S4**

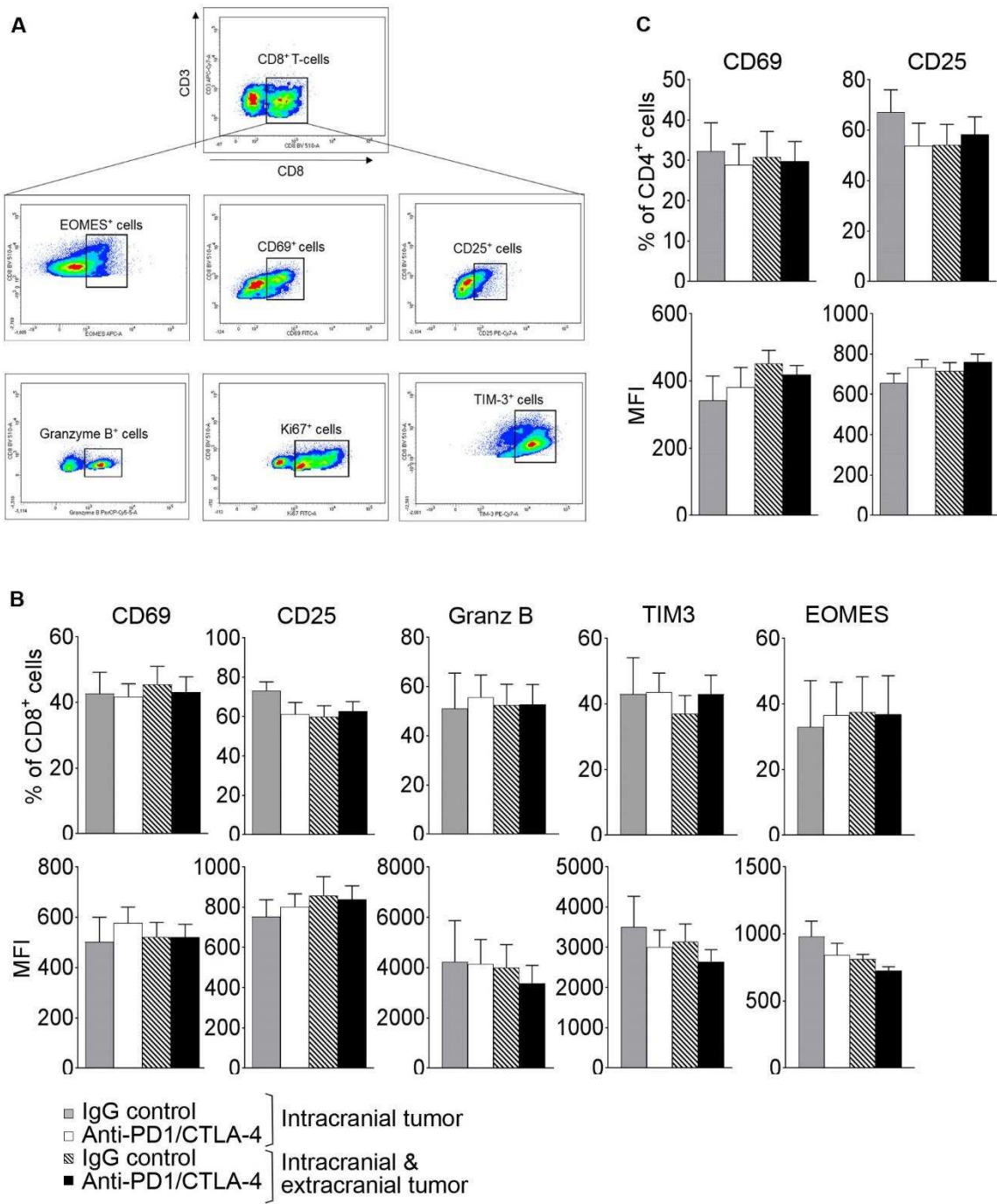


Figure S5

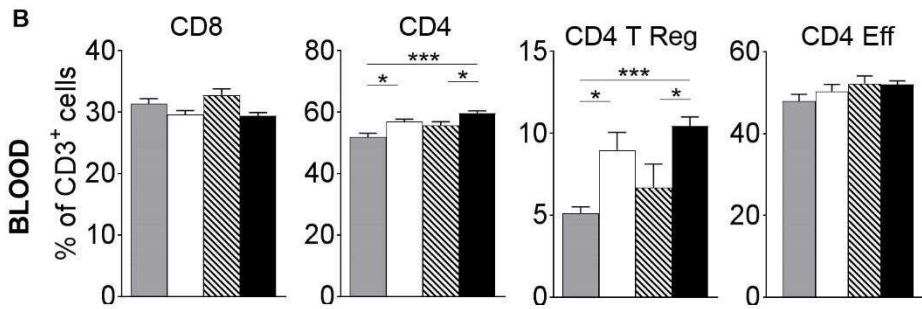
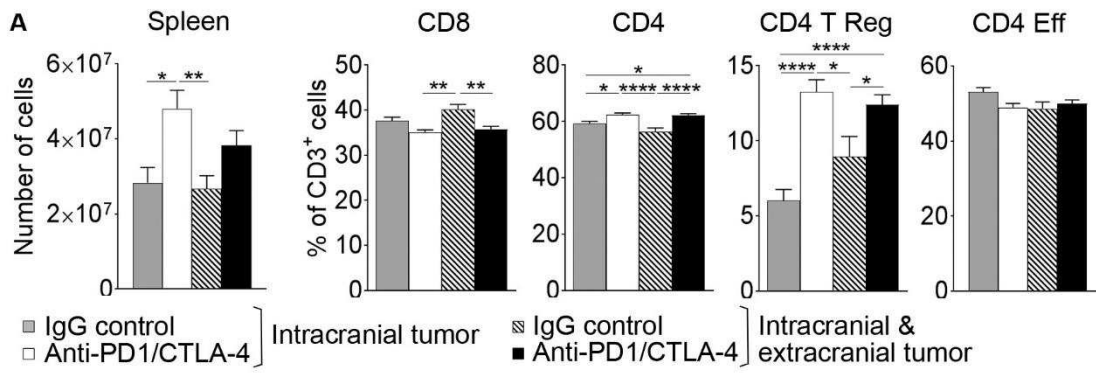


Figure S6

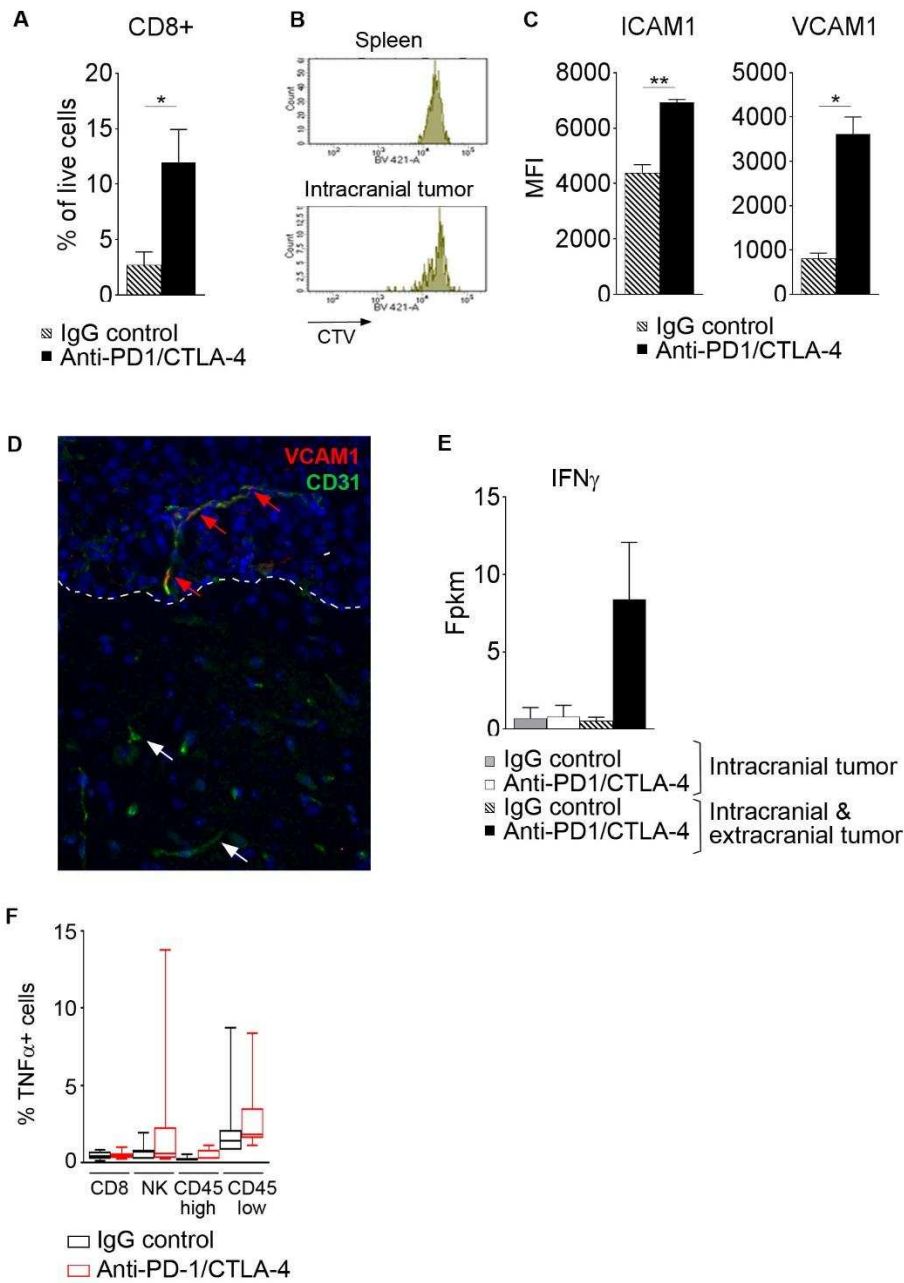


Figure S7

ANOVA parameters

Figure	Parameter	F value	DF (between columns)	DF (within columns)	DF (Total)	p value
2C	CD45	16.31	3	68	71	<0.0001
2C	CD3	13.98	3	65	68	<0.0001
2D	CD8	15.19	3	64	67	<0.0001
2D	CD4	13.27	3	34	37	<0.0001
2D	CD4 Tregs	15.00	3	34	37	<0.0001
2D	CD4 Teff	9.15	3	34	37	0.0001
2F	NK	0.44	3	66	69	0.7285
2G	Macrophages	6.99	3	68	71	0.0004
2H	Microglia	5.10	3	68	71	0.003
5A	Ki67	1.452	3	36	39	0.2438
5E	CD44+CD62L- (blood)	28.69	3	27	30	<0.0001
6D	ICAM1 (%)	20.91	3	22	25	<0.0001
6D	VCAM1 (%)	60.66	3	22	25	<0.0001
6D	ICAM1 (MFI)	47.45	3	22	25	<0.0001
6D	VCAM1 (MFI)	30.92	3	22	25	<0.0001

T-test parameters

Figure	Parameter	t-value	df	p value
5F	CD44+CD62L- (Intracr. T)	1.33	4.77	0.2422
5C	CTV+CD8+ T cells	6.78	9.26	<0.0001

Table S1